BBA - Proteins and Proteomics

Engineering of conserved residues near heavy chain complementary determining region 3 (HCDR3) improves both affinity and stability

--Manuscript Draft--

Manuscript Number:	BBAPRO-22-225R2
Article Type:	Regular Paper
Keywords:	Antibody; Antibody Engineering; Vernier Zone; Affinity-Stability trade-offs; Molecular Dynamics
Corresponding Author:	Sibel Kalyoncu İzmir Biomedicine and Genome Center TURKEY
First Author:	Merve Arslan
Order of Authors:	Merve Arslan
	Tugce Ulucay
	Seyit Kale
	Sibel Kalyoncu
Abstract:	Affinity and stability are crucial parameters in antibody development and engineering approaches. Although improvement in both metrics is desirable, trade-offs are almost unavoidable. Heavy chain complementarity determining region 3 (HCDR3) is the best-known region for antibody affinity but its impact on stability is often neglected. Here, we present a mutagenesis study of conserved residues near HCDR3 to elicit the role of this region in the affinity-stability trade-off. These key residues are positioned around the conserved salt bridge between VH-K94 and VH-D101 which is crucial for HCDR3 integrity. We show that the additional salt bridge at the stem of HCDR3 (VH-K94:VH-D101:VH-D102) has an extensive impact on this loop's conformation, therefore simultaneous improvement in both affinity and stability. We find that the disruption of π-π stacking near HCDR3 (VH-Y100E:VL-Y49) at the VH-VL interface cause an irrecoverable loss in stability even if it improves the affinity. Molecular simulations of putative rescue mutants exhibit complex and often non-additive effects. We confirm that our experimental measurements agree with the molecular dynamic simulations providing detailed insights for the spatial orientation of HCDR3. VH-V102 right next to HCDR3 salt bridge might be an ideal candidate to overcome affinity-stability trade-off.
Suggested Reviewers:	Ruth Nussinov National Institutes of Health ruth.nussinov@nih.gov She is an expert on protein molecular dynamics
	Gideon Schreiber Weizmann Institute of Science gideon.schreiber@weizmann.ac.il He is an expert on protein structure-function relationship
	Elissa Leonard Johns Hopkins University eleonar8@jhmi.edu She is an expert on antibody engineering.
	Turkan Haliloglu Boğaziçi University halilogt@boun.edu.tr She is an expert on protein-protein interfaces
	Anupam Banerjee University of Pittsburgh hoc2@pitt.edu He is an expert on protein engineering

Response to Reviewers:	All comments have been responded and uploaded as separate file.

Manuscript Number BBAPRO-22-225
Response to Reviewers (March 20th, 2023)

Dear Editor and Reviewers,

Thank you for giving us the opportunity to submit a revised draft of the manuscript "Antibody conserved residues show favorable outcomes for the affinity-stability trade-off" for publication in *Biochimica et Biophysica Acta - Proteins and Proteomics*. We appreciate the time and effort that you and the reviewers dedicated to providing feedback on our manuscript and are grateful for the insightful comments and valuable improvements to our paper.

We have incorporated most of the suggestions made by the reviewers. Those changes are highlighted within the manuscript in red font. Please see below, in blue, for a point-by-point response to the reviewers' comments and concerns. All page numbers/paragraphs/lines refer to the revised manuscript file with tracked changes.

Reviewer #1:
Arslan et al have demonstrated their work on enhancing on improving antibody affinity-stability in their manuscript entitled Conserved residues of an antibody underlie favorable outcomes for the affinity-stability trade-off". Authors claims that they successfully demonstrated the generation of stable antibody with better stability, compared to wild type using site directed mutagenesis, Dynamic scanning fluorimetry coupled with molecular dynamics in the anti-Vascular Endothelial Growth Factor (VEGF) scFv structure. To generate such stable model, that they selected a conserved salt bridge interaction (VH-K94 and D101) on the heavy chain pi-pi interacting residues (VHY100E and YL-Y49) between heavy and light chain and summaries their study the salt bridge is crucial for HCDRH3 loop conformation while the pi-pi interacting residues were crucial for the overall antibody stability. Overall, the manuscript was well written. Also, the work has been reported and presented in clear way with necessary references. Below were few minor comments for the authors to address.

1. Despite of tons of structures available in the pdb database, authors should elaborate in one or two lines what motivated to select the scFv antibody-antigen system for their work.

Author Response: We thank the referee for pointing this out. We revised our introduction text highlighting scFv format with related references in Introduction (Page 2, 2nd paragraph).

2. Consider changing the title of the manuscript, as the current one is a bit difficult to read

Author Response: We thank the referee for the suggestion. We agree that the title might be a bit complicated. Therefore, we revised our title to "Antibody conserved residues show favorable outcomes for the affinity-stability trade-off".

3. Consider removing the "developability" before parameters from line 18.

Author Response: Thanks for pointing this out. Using “developability” and “development” in the same sentence was unnecessary, so we removed it (now, line 20)

4. Consider re-phrasing “ We complement our wet-lab characterization with molecular dynamics simulations that not only confirm our measured trends but also provide detailed insight correlated with the spatial orientation of HCDR3” line 25.

Author Response: We thank the referee for this suggestion. We rephrased this part to “We confirm that our experimental measurements agree with the molecular dynamics simulations providing detailed insights for the spatial orientation of HCDR3.“ (now, line 32).

5. Line 175, Instead of "this tyrosine, consider writing Y49"

Author Response: We thank for the suggestion, we corrected it to “V_L-Y49” (now, line 193).

6. The author should check the residues numbering throughout manuscript, for example, VHD101 residue is Histidine in the deposited structure, I assume they mean VH D111, if not please fix it through out manuscript, or if authors are using Kabat annotation to label residues , consider giving alphabet numbering beside HDCRH3 residue. Also, VH 102 residue I see it as tyrosine not as a valine, VH 94 is tyrosine not lysine. Please clarify

Author Response: We thank the referee for pointing this out. We are sorry for the confusion. Kabat numbering and numbering on PDB deposited structure sometimes do not match. We added a supplementary figure (Fig. S1) aligning both deposited structure number and Kabat number of the residues. Here we utilized the web server SabPred-ANARCI (https://opig.stats.ox.ac.uk/webapps/newsabdab/sabpred/anarci/) which is a tool for numbering amino-acid sequences of antibody variable regions. We cited this tool and added related text in the Materials and Methods section (Page 4, 2nd paragraph). We updated the supplementary figure numbers in the main text and supplementary file according to this change.

7. Line 248 " instead of "experimentally produced", perhaps recombinantly produced ?

Author Response: We thank for the suggestion. We corrected this word (now, line 268).

8. They are few areas in the manuscript (abstract and introduction), which needed some language correction.

Author Response: We thank the referee for pointing this out. We re-checked and revised our abstract and introduction text and highlighted the changes.

Reviewer #3:

The manuscript describes the role of residues, mainly on HCDR3, of an antibody for the affinity and stability based on both experimental and simulation data. The results seem to be interesting, but several concerns are raised as below.

1. Anti-VEGF antibody was used to analyze the role of conserved residues. The authors should discuss the generality of results obtained for anti-VEGF antibody.

Author Response: We thank the referee for this suggestion. All the domains of antibody heavy and light chains share the same structural conformation called “immunoglobulin fold”. This fold is mainly specified with anti-parallel β-sheets and loops. Besides, the salt bridge we focused on is very conserved among all organisms. Please see below for amino acid distributions of all organisms on positions 94 and 101 (salt bridge forming residues). (http://www.abysis.org/abysis/searches/distributions/distributions.cgi). Here, positions 94 and 101 within the heavy chain have 81% of positively charged amino acids (K + R) and 79% of negatively charged amino acids (D+E), respectively. Those findings support the applicability of the results and the designs we used to other antibodies. We revised our discussion text according to these findings and highlighted these changes (line 466 – 468).

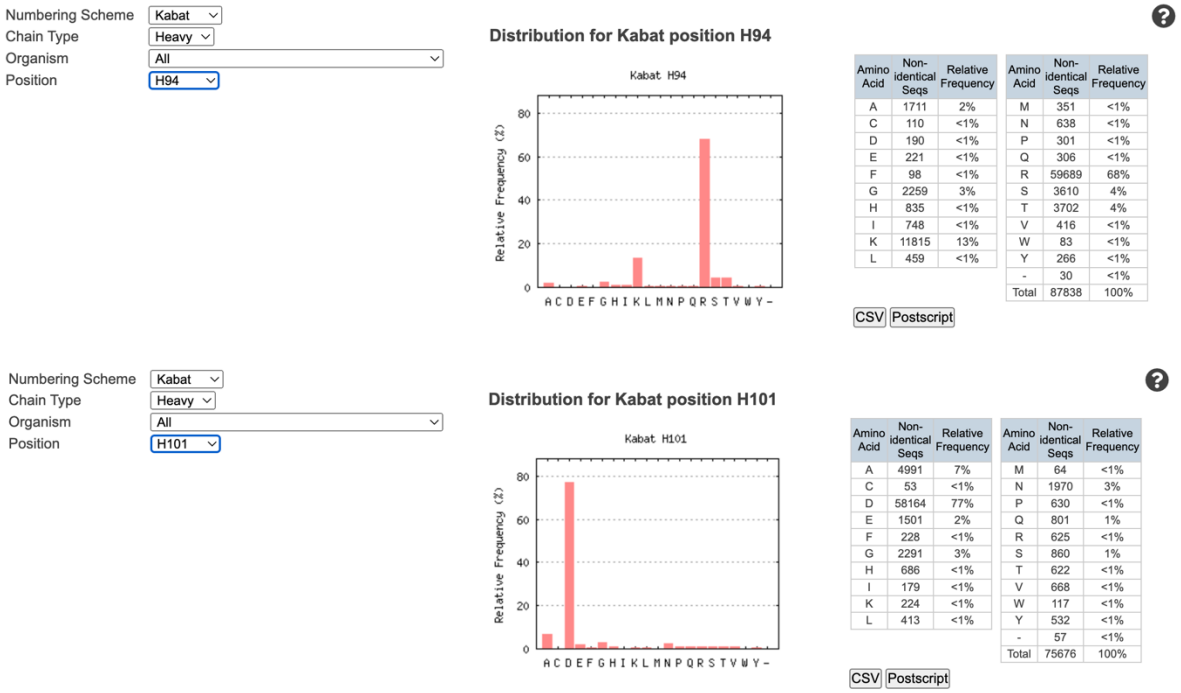

Amino Acid	Non-identical Seqs	Relative Frequency
A	1711	2%
C	110	<1%
D	190	<1%
E	221	<1%
F	98	<1%
G	2259	3%
H	835	<1%
I	748	<1%
K	11815	13%
L	459	<1%
M	351	<1%
N	638	<1%
P	301	<1%
Q	306	<1%
R	59689	68%
S	3610	4%
T	3702	4%
V	416	<1%
W	83	<1%
Y	266	<1%
-	30	<1%
Total	87838	100%

Amino Acid	Non-identical Seqs	Relative Frequency
A	4991	7%
C	53	<1%
D	58164	77%
E	1501	2%
F	228	<1%
G	2291	3%
H	686	<1%
I	179	<1%
K	224	<1%
L	413	<1%
M	64	<1%
N	1970	3%
P	630	<1%
Q	801	1%
R	625	<1%
S	860	1%
T	622	<1%
V	668	<1%
W	117	<1%
Y	532	<1%
-	57	<1%
Total	75676	100%

2. The authors should comment on the residues whether they change or not change on the affinity maturation process. On the affinity maturation, the affinity increases. Then, how about the stability?

Author Response: We thank the referee for this suggestion. We added a comment in our discussion text (line 460-461).

3. The authors should check whether the scFvs fold correctly. Secondary structure analysis using circular dichroism would be needed.

Author Response: We thank the referee for pointing this out. V_L-Y49 is placed within the β-sheet while V_H-V102 is placed within the loop in the deposit structure. Because we did not have a CD instrument in our laboratory use, we assessed the effect of point mutations in *in silico* secondary structure prediction tool (http://sable.cchmc.org/). These predictions show that the secondary structure of the scFvs seem to tolerate single point mutations when we compared mutated scFv predictions with WT prediction. We added these in the method section with a title "In silico secondary structure prediction" (line 141-145), shared the results in Supplementary Figure 6, and mentioned it in the Result section (line 251-252). We updated the supplementary figure numbers in main text and supplementary file according to this change.

4. For protein concentration determination, molecular coefficient should be described.

Author Response: We thank the referee for pointing this out. We have added the molecular coefficients of the proteins in the materials and methods section (line 168-170).

5. For SPR experiments, regeneration methods should be described.

Author Response: We are sorry for omitting this important information. We added the regeneration method details in the materials and methods section (line 183-184).

Antibody conserved residues show favorable outcomes for the affinity-stability trade-off

Merve Arslan [1,2,†], Tuğçe Uluçay [1, †], Seyit Kale [1], Sibel Kalyoncu [1,*]

[1] Izmir Biomedicine and Genome Center, 35340 Balçova, Izmir, Turkey

[2] Izmir International Biomedicine and Genome Institute, Dokuz Eylul University, 35340 Balçova, Izmir, Turkey

[†] The authors wish it to be known that, in their opinion, the first two authors should be regarded as joint First Authors.

*** Corresponding author:**
Sibel Kalyoncu

Izmir Biomedicine and Genome Center, 35340 Balçova, Izmir, Turkey

Email: sibel.kalyoncu@ibg.edu.tr

Phone: +90 232 4126567

Highlights

- Antibodies are effective in treating various diseases due to many advantages.
- Having insights on antibody structure-function is key for antibody development.
- Mutations on conserved regions can be critical for the antibody developability.
- Antibody affinity-stability trade-offs can be overcome by the help of conserved residues.

Engineering of conserved residues near heavy chain complementary determining region 3 (HCDR3) improves both affinity and stability

Merve Arslan [1,2,†], Tuğçe Uluçay [1, †], Seyit Kale [1], Sibel Kalyoncu [1,*]

[1] Izmir Biomedicine and Genome Center, 35340 Balçova, Izmir, Turkey

[2] Izmir International Biomedicine and Genome Institute, Dokuz Eylul University, 35340 Balçova, Izmir, Turkey

[†] The authors wish it to be known that, in their opinion, the first two authors should be regarded as joint First Authors.

*** Corresponding author:**
Sibel Kalyoncu

Izmir Biomedicine and Genome Center, 35340 Balçova, Izmir, Turkey

Email: sibel.kalyoncu@ibg.edu.tr

Phone: +90 232 4126567

Abstract

Affinity and stability are crucial parameters in antibody development and engineering approaches. Although improvement in both metrics is desirable, trade-offs are almost unavoidable. Heavy chain complementarity determining region 3 (HCDR3) is the best-known region for antibody affinity but its impact on stability is often neglected. Here, we present a mutagenesis study of conserved residues near HCDR3 to elicit the role of this region in the affinity-stability trade-off. These key residues are positioned around the conserved salt bridge between V_H-K94 and V_H-D101 which is crucial for HCDR3 integrity. We show that the additional salt bridge at the stem of HCDR3 (V_H-K94:V_H-D101:V_H-D102) has an extensive impact on this loop's conformation, therefore simultaneous improvement in both affinity and stability. We find that the disruption of π-π stacking near HCDR3 (V_H-Y100E:V_L-Y49) at the V_H-V_L interface cause an irrecoverable loss in stability even if it improves the affinity. Molecular simulations of putative rescue mutants exhibit complex and often non-additive effects. We confirm that our experimental measurements agree with the molecular dynamic simulations providing detailed insights for the spatial orientation of HCDR3. V_H-V102 right next to HCDR3 salt bridge might be an ideal candidate to overcome affinity-stability trade-off.

Keywords: Antibody, Antibody Engineering, Vernier Zone, Affinity-Stability trade-offs, Molecular Dynamics

Introduction

Antibodies are widely utilized as diagnostics and therapeutics tools thanks to their high affinity and specificity toward target antigens. Hundreds of therapeutic antibodies in different formats such as Fab, single-chain variable fragment (scFv), or nanobodies, continue being developed and tested in clinical trials [1, 2]. Due to their small size, monovalent nature, and simpler folding paths [3] , scFvs offer several beneficial attributes for *in silico* and *in vitro* developability applications [4-6] . Although scFvs might show some drawbacks such as lower stability, and fast clearance, they are readily suitable for protein engineering strategies to overcome them [7, 8] .The eventual success of the antibody depend strongly on its developability properties such as activity and stability. The activity of an antibody is related to its strong and specific binding to its cognate antigen, a metric that is known as *antigen affinity* [9]. A molecular-level understanding of the affinity is ~~a~~ challenging, that might limit antibody development. Affinity improvement efforts can result in detrimental effects on the overall profile [10, 11]. The primary bottleneck here is *stability* which is another important developability parameter often negatively correlated with the affinity [12-14]. For a successful antibody, it is critical to maintaining a necessary level of stability while engineering the affinity. Thus, co-screening of stability and affinity is essential to find the optimal mutations [15, 16].

Affinity modulation efforts have historically focused on the complementarity determining regions (CDRs), particularly heavy chain CDR3 (HCDR3) [17, 18]. These regions are intrinsically *hypervariable* originating from somatic hypermutations in mature B cells which leads to CDR sequence diversity [19]. Several studies point out that non-CDR regions (known as framework residues) can also be important for affinity because they impact the overall antibody structure [11, 20, 21]. Affinity gains by substitutions of non-CDR residues have been generally underestimated in directed evolution strategies. And there has been little systematic study to assess the consequences of this bias. In this context, one of the non-CDR regions is the Vernier zone [22]. The Vernier zone of an antibody is characterized by a set of critical framework residues underlying the CDRs [23, 24]. These residues potentially affect the conformations of the CDR loops and their orientation with respect to the antigen epitope; thus, they are common targets of humanization efforts to regain affinity via back mutations [22, 25, 26]. Roles of the

Vernier zone region on other antibody properties such as specificity and stability remain to be elucidated [27].

Powerful experimental technologies such as directed evolution and rational designs have made *in vitro* evolution of antibodies more efficient and have taken the field of modern antibody engineering further [28]. While experimental approaches can generally provide reliable results, scalability can be cumbersome, labor-intensive, and prohibitively expensive [29]. In this context, *in silico* approaches can provide invaluable opportunities with their high-throughput potential and ready access to atomic-level details [30]. Molecular dynamics (MD) simulations investigate the biomolecular structures of antibodies at their natural dynamics on timescales relevant to their physiological function. These efforts can provide critical supporting information, including (i) computed free energy differences and measured forces behind protein-protein binding [31, 32], (ii) atomic-level dynamics, (iii) information about protein stability in different physiological and experimental conditions [33-35] and (iv) the nature of the interactions between an antibody and its cognate antigen [36]. MD methods combined with rational design approaches can be used to design better antibodies in a shorter time, with improved accuracy and at a reduced cost [37]. The number of successful examples of this approach published in literature is on the rise [38-43].

In this study, we generated rationally chosen mutations on an anti-Vascular Endothelial Growth Factor (VEGF) scFv to investigate their effects on affinity and stability. Salt bridges are one of the most critical non-covalent forces in protein structure and function [44]. The salt bridge between the two heavy-chain residues 94 and 101 (according to Kabat numbering) is a highly conserved structural motif that supports the robust shape of HCDR3 [45, 46]. Modifying or altering this interaction is virtually always detrimental for both stability and affinity [47]. Motivated by this critical observation, we hypothesized that the vicinity of this salt bridge is a natural starting point to investigate the trade-off between affinity and stability. To this end, we generated an anti-VEGF scFv antibody [48] and designed mutations in both heavy chain (V_H) and light chain (V_L) sides of this salt bridge accompanying the Vernier zone residues around (**Figure 1A**). Anti-VEGF antibodies are successful anti-cancer therapeutics [49] and thanks to its universal nature of the Vernier zone, the lessons learned in this study could be transferable to other antibodies in general. We performed both comparative molecular dynamics simulations and experimental characterizations to gain a molecular-level understanding of the factors that modulate this trade-off. We found that existing and *de novo* secondary/tertiary interactions around this HCDR3 salt bridge are a critical determinant of both antigen binding and the robustness of the V_H-V_L interface, thus playing a crucial and complex role in the co-evolution of affinity-stability. Our overall findings obtained from our experimental and MD studies show the importance of joint efforts to elucidate the molecular mechanisms of antibody design.

Materials and Methods

Setup Preparation and analysis of Molecular Dynamics Simulations

Atomic coordinates of the anti-VEGF scFv antibody fragment were taken from the Protein Data Bank (PDB ID:1BJ1; chains H, L and W) [50]. Constant fragment groups and the linker between the variable groups were omitted. When scFv linker length is longer than 12 residues, covalently linked V_H and V_L form a functional and monomeric scFv [51-53] and it was previously shown that absence of linker do not affect calculated distributions of molecular dynamic simulations [54]. Amino acid distributions of each Kabat numbering positions were extracted from AbYsis database (www.abysis.org). Mutant constructs were prepared using the Wizard Mutagenesis tool of PyMOL

Molecular Graphics System, version 2.1.1, Schrödinger LLC. Each antibody-antigen complex is solvated in a cubic water box that is sufficiently large to provide a minimum buffer zone of 12 Å between biological material and the cubic system boundaries. Na^+ and Cl^- ions were placed randomly to neutralize the system electrostatically at a physiological salt concentration of 0.150 M. CHARMM36m force field [55, 56] was chosen together with the four-site OPC water model [57] subject to periodic boundary conditions. A combination of conjugate gradient and steepest descent methods were applied for initial energy minimization. Later, the system was equilibrated in the NVT ensemble at 100K for 1 ns, and at 310K for 1 ns, both using a small integration time step of 1 fs. Production trajectories were collected in the NPT ensemble at 310K and 1 atm atmospheric pressure using a 2 fs of integration time steps for a total of 500 ns. Atomic coordinates were saved every 100 ps.

Kabat numbering scheme and the domain definitions were used to determine complementarity-determining regions (CDRs) and the frameworks (FWs) [58, 59] utilizing the web server SabPred-Anarci [60]. Since there are some differences between the Kabat number of the residues and the deposited structure number of the residues, the alignments of the numbering schemes were presented in **Supplementary Figure 1.** The contacts and distances between V_H and V_L chains were utilized to assess stabilities, the contacts and distance between both antibody chains and the antigen for affinities. A contact between two interacting domains was defined geometrically for when two heavy (i.e., non-hydrogen) atoms are close to each other within a cutoff of 5 Å or less. Contacts were averaged over all recorded molecular configurations in each trajectory (5000 frames for each simulation). The proximity between two given residues was calculated by the distance between the centers of mass of interacting atoms of given residues. Root mean square fluctuations (RMSFs) were calculated based on the α-carbons of protein chains. The area of the V_H-V_L interface is calculated by subtracting the solvent-accessible surface area (SASA) of the complexed V_H-V_L pair from the sum of the SASAs of the individual V_H and V_L domains. Mass centers, per residue RMSFs, SASA computations were performed by VMD-Python library (https://vmd.robinbetz.com/), and distances between the centers were computed by Python's Numpy. Gromacs version 2018.3 [61] was used for all simulation setups and for the collection of trajectories. VMD [62] and in-house Python scripts were used for all analyses and visualizations.

In silico secondary structure prediction

The secondary structure of the wild-type and all mutant antibodies were predicted via SABLE prediction webserver [63]. One letter amino acid codes of the antibody sequences were used as input separately. Secondary structure was chosen for prediction goal, SABLE II was chosen for server version, WApproximator was chosen for predictor type.

Protein constructs and protein expression

The anti-VEGF single chain antibody fragment (scFv) heavy chain (V_H) and light chain (V_L) fused via a 21 amino acids length non-repetitive linker "SPNSASHSGSAPQTSSAPGSQ" [53]. The scFv mutants were generated by QuikChange Lightning Site-Directed Mutagenesis Kit (Agilent). The scFv mutants with the leader sequence (PelB), FLAG-tag and polyhistidine-tag were transformed into *E.coli* strain BL21 (DE3) pLysS (Thermo Fisher) with pET17-b (GenScript) expression plasmid. Transformant cells were grown on LB-agar plates containing 100µg/mL ampicillin and 25µg/mL chloramphenicol. Single colonies were inoculated in LB broth containing 100µg/mL ampicillin and 25µg/mL chloramphenicol and grown overnight at 225 rpm, 37 °C. These cells were inoculated into 300 mL autoinduction-media and incubated at 18°C, 250 rpm for 48 h [64].

Protein purification

Cultures were centrifuged at 6500xg and 4°C (Avanti, Beckman Coulter). Protein containing supernatant was incubated with His-Pur Ni-NTA resin (Thermo Fisher) for 2 h at 4°C shaking vigorously. The mixture was loaded into a 10 ml vacuum column (Thermo Fisher) and purified according to recommended commercial protocol. Phosphate buffered saline (PBS) with 25 mM Imidazole, pH 7.4 and PBS with 500 mM Imidazole, pH 7.4 were used as wash and elution buffers, respectively. Purified protein was buffer-exchanged into PBS (pH 7.4) through membrane filtration (Amicon® Ultra-4 Centrifugal Filter Units, MWCO 10 kDa, Merck). Protein samples were loaded onto HiTrap ™ Protein L column (GE Healthcare) as a second purification step to maximize protein purity. Protein purities were confirmed on sodium dodecyl sulfate-polyacrylamide gel electrophoresis analysis (TGX ™, FastCast™, 12% Acrylamide kit; Bio-Rad). Precision Plus Protein™ Dual Color standard was used as a marker (Bio-Rad). Protein concentrations were determined by NanoDrop 2000 (at 280 nm). Extinction coefficients were determined 68550 M^{-1} cm^{-1} for WT and V_H-V102D, 67060 M^{-1} cm^{-1} for V_L-Y49D, V_L-Y49K, V_L-Y49N, 70040 M^{-1} cm^{-1} for V_H-V102Y via Expasy ProtParam webserver while using the protein sequences as input [65].

Thermal denaturation assay

Thermal unfolding profiles of purified scFv proteins were determined by thermal shift assay by ABI 7500 Fast RT-PCR. SYPRO™ Orange Protein Gel Stain (Thermo Fisher) at 5x concentration was used with a 5 µM antibody concentration. Temperature range of 25-99°C with a 0.05% ramp rate was used. Thermal transition mid-points (i.e., T_m values) from the thermogram data were determined using the Hill equation fit by Origin 8.5 software.

Surface Plasmon Resonance (SPR)

Affinity measurements were performed using surface plasmon resonance (SPR) on a Biacore T200 instrument (Biacore Inc., Piscataway, NJ). All experiments were performed in an HBS-EP buffer, pH 7.4. 1000 nM His-tagged VEGF protein was immobilized on a CM4 chip at a flow rate of 10 µl/min for ~1 min (target RU for immobilization was 100 RU). A series of solutions ranging from 10 to 100 nM scFv fragments were subsequently injected at a flow rate of 30 µl/min onto the VEGF-immobilized surface. Regeneration was performed with 10 mM glycine-HCl at pH 2.7 at a flow rate of 30 µl/min for 30 seconds after each concentration in the run. Data were corrected by double-referencing against a control flow cell containing no VEGF and injecting buffer solution. Sensogram curves were analyzed using the BiaEval 3.0 manufacturer's software. K_D, k_{on} and k_{off} values were calculated by fitting the kinetic association and dissociation curves to a 1:1 binding model.

Results

Rationale behind mutational designs

Two positions, one from light chain (V_L-Y49) and one from heavy chain (V_H-V102) are chosen to evaluate affinity/stability trade-offs through secondary interactions of the conserved salt bridge (V_H-K94 and V_H-D101) under the stem of HCDR3. V_L-Y49 is a conserved framework residue which is positioned at the V_L-HCDR3 interface. V_L-Y49 makes π-π contacts with an HCDR3 residue, V_H-Y100E. On the other hand, V_H-Y100E makes an either hydrophobic or anion-π contact with V_H-D101 [66], so there is an anion-π-π interaction between those three residues (V_H-D101:V_H-Y100E:V_L-Y49, **Figure 1A**). For V_L-Y49, we designed three mutations, Y49N to evaluate anion-π-amino interaction, Y49K to evaluate anion-π-cation interaction and Y49D, anion-π-anion interaction.

Because this position is surface accessible, all these mutations would also help to improve solubility leading to a possible stability increase. However, Y49D mutation is designed as disruptive mutation due to possibility of repulse between two negatively charged amino acids, V_L-D49:V_H-D101.

V_H-V102 is the last residue of HCDR3, does not have contacts with antigen and it is relatively conserved according to its distribution in *Homo sapiens* (**Supplementary Figure 5)**. The most common residue is tyrosine (33%) followed by valine (24%). This residue is also highlighted as one of the key stabilizing contacts for HCDR3 structural diversity [46]. On the other hand, aspartate in this position is rarely found (1%). We designed two mutations for this position: V_H-V102Y and V_H-V102D. While V_H-V102Y would show the difference between the two most conserved amino acids, V_H-V102D might form complex salt bridge at the stem of HCDR3 and it might also improve stability in soluble conditions due to its negative charge.

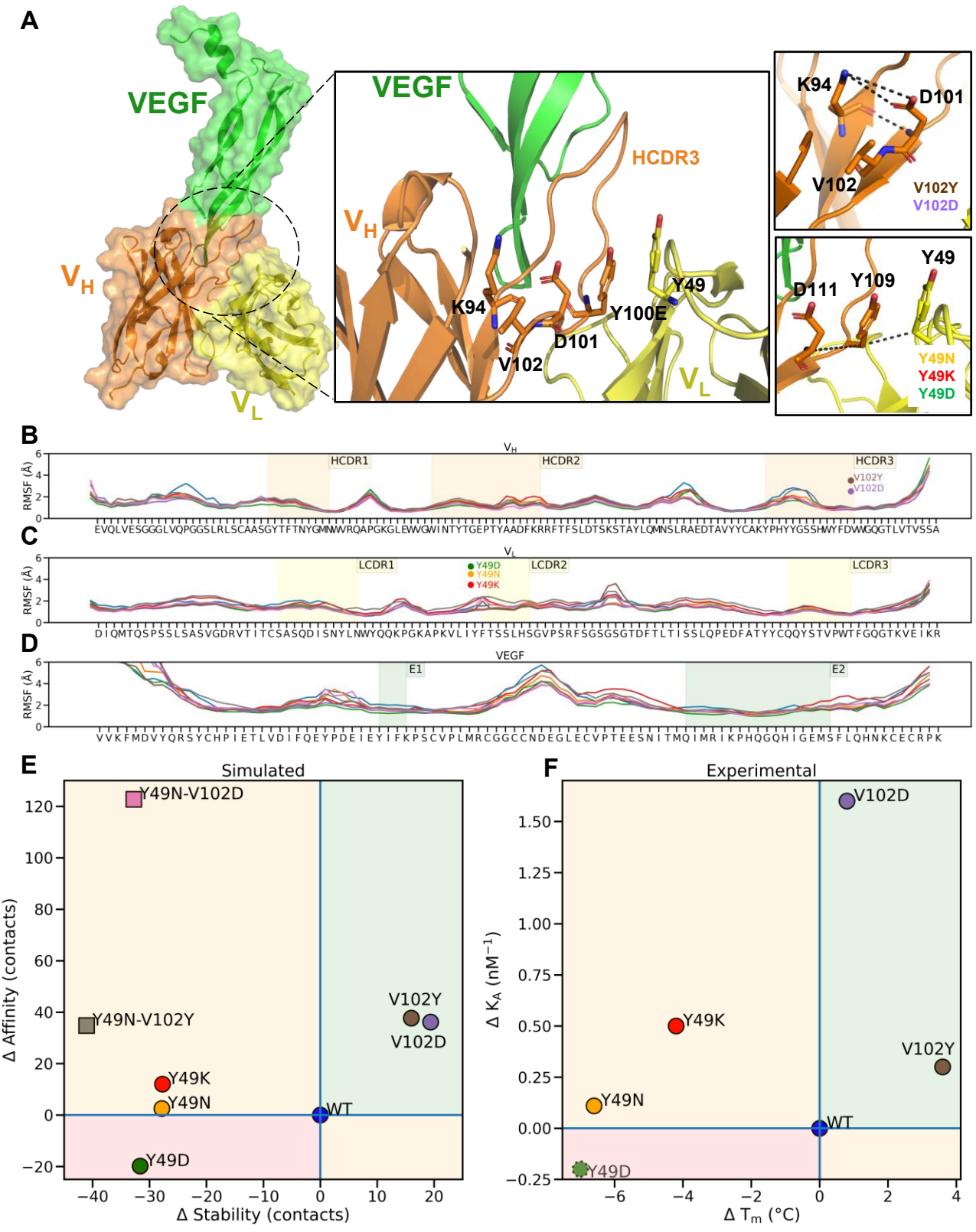

Figure 1: Mutations in the vicinity of the conserved salt bridge (V_H-K94:V_H-D101) of the variable heavy chain modulate antibody affinity and stability characteristics. **(A)** View of the antigen (Vascular Endothelial Growth Factor, VEGF) bound to its cognate scFv fragment (left panel, PBD

ID: 1BJ1 [50]). Insets show the salt bridge as well as the nearby mutational landscape investigated in this study (center and right panels, respectively). Orange, yellow, and green colors indicate the scFv heavy chain (V_H), scFv light chain (V_L) and VEGF proteins, respectively. The conserved salt bridge between V_H residues K94 and D101 is indicated via dashed black lines (top right panel). Rational mutations on scFv involve residues V102 (on V_H) and Y49 (on V_L). **(B-D)** Molecular dynamics of the wild-type (WT) and mutated scFv constructs. The flexibility of the proteins are illustrated by the average root mean square fluctuations (RMSFs) of backbone atoms of the heavy chain **(B)**, the light chain **(C)** and the antigen VEGF **(D)**. Blue, orange, red, green, brown, purple, pink and gray lines indicate WT, V_L-Y49N, V_L-Y49K, V_L-Y49D, V_H-V102Y, V_H-V102D, V_L-Y49N-V_H-V102D, V_L-Y49N-V_H-V102Y mutants, respectively. This color convention is used throughout the rest of the text. Complementarity determining regions (CDRs) of the heavy chain, the light chain and the epitopes of VEGF are highlighted in orange, yellow and green, respectively. Mutated residues are annotated with circles. The time evolution of the V_H:V_L contacts for all mutants are shown in **Supplementary Figure 2**. The time evolution of the antibody:antigen contacts for all mutants are shown in **Supplementary Figure 3. (E-F)** Scatter plots of affinity and stability differentials with respect to the WT antibody. The green areas represent "increased affinity and increased stability", red "decreased affinity and decreased stability" and oranges "decreased affinity or stability", meaning a trade-off. **(E)** Computed contact differentials from the molecular dynamics trajectories (See Methods). Differences in the mean of total contact counts between the V_H and V_L chains (an indicator of stability, x-axis) and between scFv and VEGF (an indicator of affinity, y-axis) with respect to their WT counterparts are shown. Distribution of contact counts between VH:VL (stability) and antibody antigen (affinity) are shown in **Supplementary Figure 4A and 4B**, respectively. **(F)** Experimentally measured stability (T_m, thermal melting temperature, x-axis) and affinity (as illustrated via $K_A = 1/K_D$, the association constant, y-axis) differentials of each mutant with respect to the WT. The experimentally unstable construct V_L -Y49D is annotated via a dashed-edged circle. Considering their discouraging MD properties, we did not attempt to produce the two double mutants (V_L-Y49N-V_H-V102D, V_L-Y49N-V_H-V102Y) (square marks in **E**).

Affinity and stability profiles of designed scFvs

The conserved salt bridge between V_H-K94:V_H-D101 at the stem of HCDR3 defines the robustness of this loop (**Supplementary Figure 5)**. HCDR3 is the main paratope for most antigens [67], thus we designed several mutations around this salt bridge, preferentially on a Vernier zone residue. We aimed to modulate the antigen affinity without compromising HCDR3 because it is critical that the stem of HCDR3 has a light-chain interface that can contribute to the stability of the antibody. We chose residues V_H-V102 and V_L-Y49 to understand the secondary/tertiary effects on the V_H-V_L interface (**Figure 1A**). In the MD simulations of these constructs, average root means square fluctuations (RMSF) values near the mutations remained within the range of 6 to 10 Å, indicating that the antibody and antigen structures can still maintain a robust binding configuration. These results suggest that the overall structural flexibility of scFvs is not altered significantly by the introduced mutations **(Figure 1B-D)**. *In silico* secondary structure predictions also showed that point mutations are well tolerated within scFv secondary structure **(Supplementary Figure 6)**. However, the conserved or drastic mutations on V_H-V102 and V_L-Y49 revealed notable affinity and/or stability changes [68] (**Figure 1B-F, Figure 2**).

On the V_H side, while V_H-V102Y is a mutation to a more conserved residue for this specific position (33% Y, 24% V, **Supplementary Figure 5)**, V_H-V102D mutation is a drastic change to see whether the ionic bonding of the salt bridge at the stem of HCDR3 is disrupted by the introduction of a proximal acidic residue. Both mutations improve affinity and stability as suggested jointly by our

MD simulations and experimental measurements (**Figure 1E, F, Figure 2**). Only V102D has a higher than predicted affinity while showing slight difference in stability.

HCDR3 is in direct contact with the V_L chain through the V_H-Y100E:V_L-Y49 π-π interaction (**Figure 1A**). Although V_H-Y100E is in HCDR3, this π-π stacking proves to be a crucial contact for the V_H-V_L interface and the HCDR3 robustness through V_H-D101:V_H-Y100E:V_L-Y49 anion-π-π stacking. We designed V_L-Y49K, V_L-Y49N and V_L-Y49D mutations to convert this triple stacking into anion-π-cation, anion-π-amino and anion-π-anion, respectively. Here, we designed the V_L-Y49D mutant as a negative control to disrupt this stacking interaction and we showed that it has very low stability according to MD simulations. Probably related to this stability loss, it even could not be recombinantly produced (**Figure 1E, F**). The other mutants were successfully produced and purified from the supernatant (**Figure 2A**). Among the mutants, V_H-V102Y showed the highest increase in thermal stability while V_H-V102D mutant improved the thermal stability slightly compared to WT (**Figure 2C**). Those two mutants also showed improved affinity in SPR analysis (**Figure 2B, Supplementary Figure 7)**. Although V_L-Y49N, V_L-Y49K mutations showed slightly increased affinity, their stability is compromised according to both computational and experimental findings (**Figure 1B-F, Figure 2B-C, Supplementary Figure 7)**.

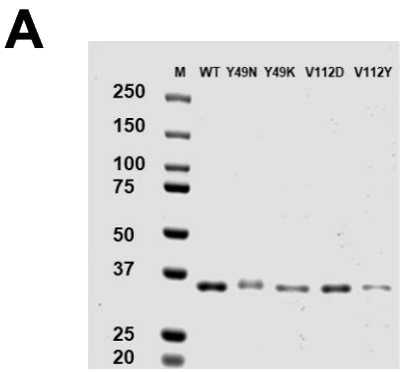

B

	T_m (°C)	K_D (nM)
WT	51.0 ± 0.4	2.51 ± 0.01
Y49N	44.4 ± 0.1	1.96 ± 0.11
Y49K	46.8 ± 0.2	1.09 ± 0.08
V102Y	54.6 ± 0.4	1.42 ± 0.03
V102D	51.8 ± 0.1	0.50 ± 0.01

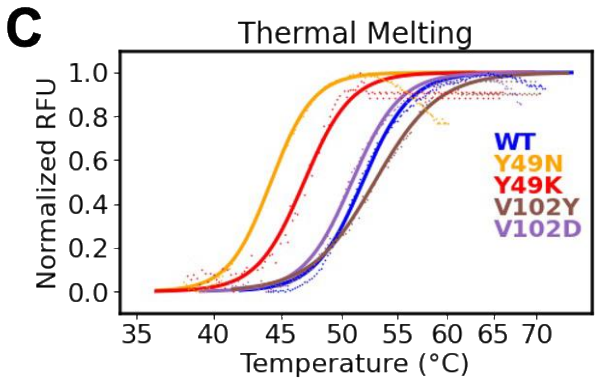

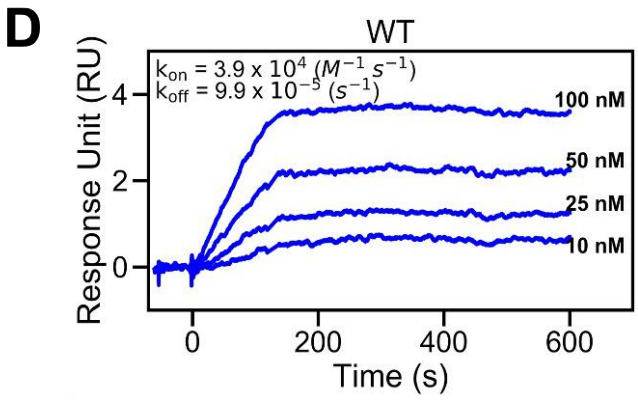

Figure 2. Experimental affinity and stability profiles of scFv constructs in this study. **(A)** SDS-PAGE analysis of scFvs after bacterial expression and purification, **(B)** Thermal melting temperature (T_m, in degrees) and dissociation constant (K_D, in molarity units) values, **(C)** T_m plots (repeated at least two times in three replicates with different batches of protein) **(D)** SPR profile of WT for affinity determination (SPR profiles of all mutants are in **Supplementary Figure 7)**. Color coding follows Figure 1.

Rescue mutations have non-additive effects

To restore the stability loss of V_L-Y49N by the stability-favoring mutations (V_H-V102D and V_H-V102Y), we designed two *in silico* double mutants, V_L-Y49N:V_H-V102D and V_L-Y49N:V_H-V102Y. Surprisingly, both rescue mutants showed even worse stability profiles as observed in the MD simulations (**Figure 1E**). As a result, we did not pursue these mutants experimentally. Most importantly, this finding shows that the effects of single point mutations are not additive and more complex secondary/tertiary interactions are at play for affinity/stability profiles. We tried to have an insight into the affinity/stability profiles of our designed mutants through more detailed structural studies.

HCDR3 is essential for both affinity and stability

Computed pairwise contact counts between the protein components of V_L-Y49N suggested specific regions for the increase in affinity and the loss in stability (**Figure 3**). While the affinity gain is mostly due to HCDR3-VEGF contact increase as expected, stability decrease is mostly caused by V_H-V_L interface disruption through HCDR3, LCDR3 and/or light framework 2 (LFW2) contact loss (**Figure 3A, B**). As expected, VEGF binding occurs mostly with V_H chain (**Figure 3C**). Same regions (HCDR3-VEGF for affinity, HCDR3, LCDR3 and LFW2 for stability) play similar roles in other mutants (**Supplementary Figures 8-13)**. Although V_H-V102Y and V_H-V102D mutants are not directly in the V_H-V_L interface, they have a drastic stability increase probably due to secondary HCDR3 interactions and/or stronger intra-HCDR3 contacts. We can examine the HCDR3 loop on two sides, one face to VEGF (HCDR3 residues 95-100B) that play roles in binding and shows mostly change in VEGF binding, while the other face (HCDR3 residues 100B-102) shows changes in V_L interacting surface (**Figure 1A**). This emphasizes that HCDR3 has crucial roles in both affinity and stability profiles of antibodies.

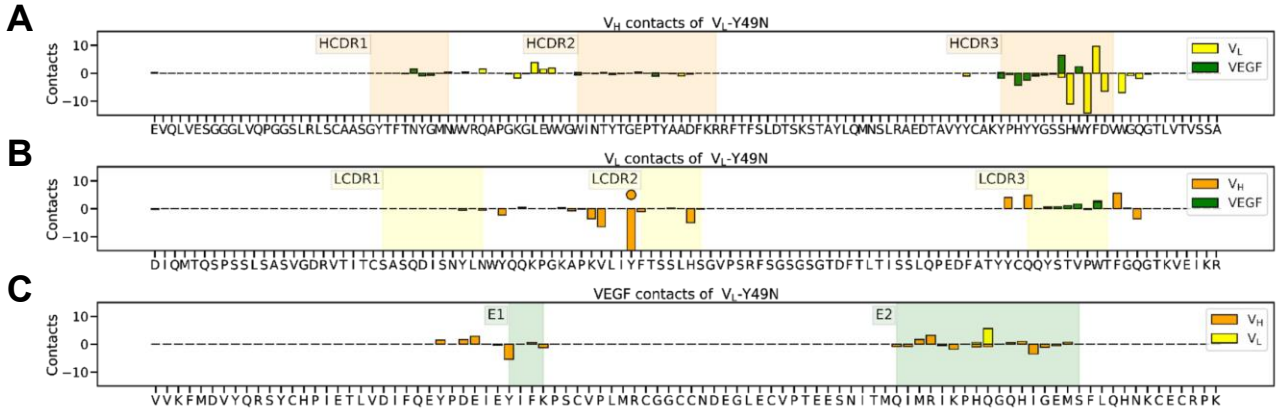

Figure 3. Difference in pairwise contact counts of V_L-Y49N mutant with respect to WT. V_H, V_L and VEGF interactions per residue are colored orange, yellow and green, respectively. **(A)** V_L and VEGF contact count differences for V_H residues. **(B)** V_H and VEGF contact count differences for V_L residues. Mutated residue is annotated with a circle. **(C)** V_H and V_L contact count differences for VEGF residues. FW regions are not shown: FW1 is before CDR1, FW2 is in between CDR1-CDR2, FW3 is in between CDR2-CDR3, FW4 is in after CDR3. Color coding follows Figure 1.

V_H-V_L interface is compromised in low-stability mutants

The V_H-V_L interface and its packing are known to have a significant effect on the stability of an antibody [69, 70]. We analyzed the V_H-V_L interface by computing the buried surface areas (BSAs) of each mutant (**Figure 4, Supplementary Figure 14)**. We calculated this property by subtracting solvent accessible surface area (SASA) of the complete V_H-V_L complexes from the sum of the SASAs of the individual V_H/V_L proteins (**Figure 4A**). Mutants with high measured thermal melting points (V_H-V102Y, V_H-V102D) also have computed BSA values close to or higher than that of the WT (~1750 Å^2 or higher). On the other hand, mutants with low measured thermal melting points (V_L-Y49N, V_L-Y49K, V_L-Y49D) also have computed BSA values that are less than of that of the WT (lower than 1700 Å^2, **Figure 4B**).

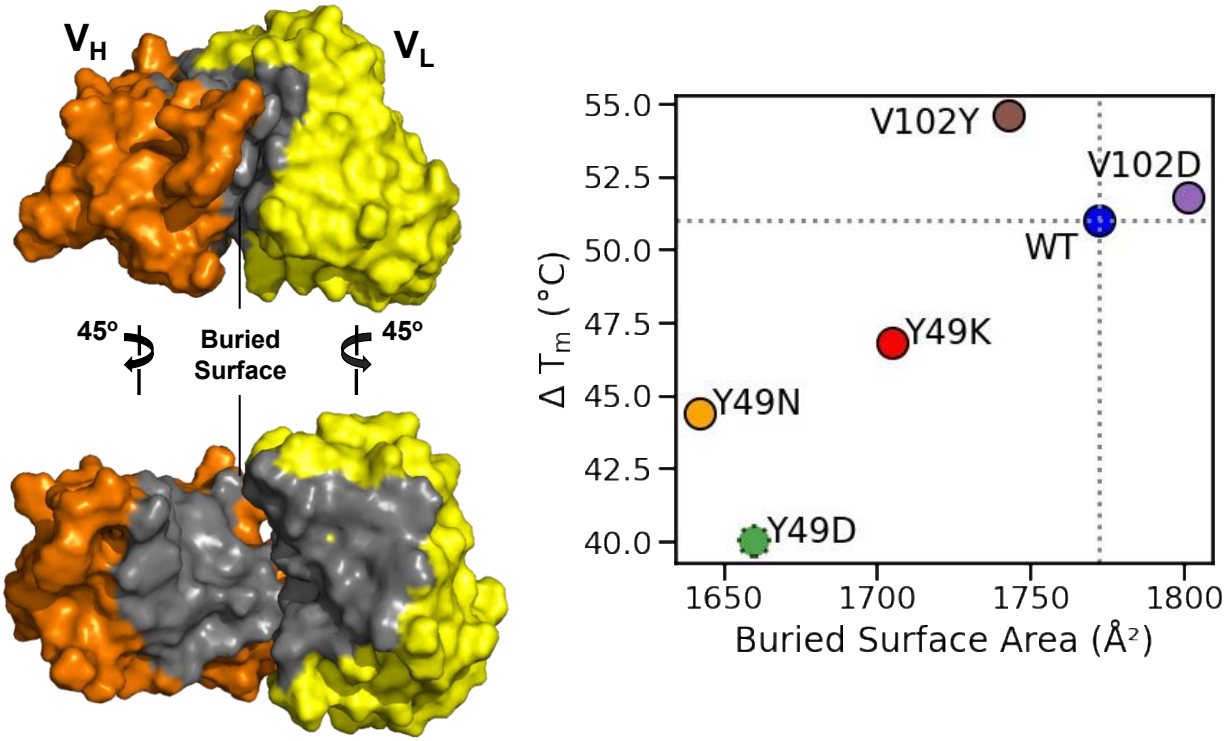

Figure 4: Correlation between measured thermal stabilities and computed V_H-V_L buried surface areas of all mutants. The area of the V_H-V_L interface is calculated by subtracting the solvent-accessible surface area (SASA) of the complexed V_H-V_L pair from the sum of the SASAs of the individual V_H and V_L domains. **(A)** Surface representation of the calculated buried surface area. Surfaces of V_H, V_L and their buried surface areas are colored orange, yellow and gray, respectively. **(B)** Computed average buried surface areas are scattered with the experimental melting temperature values (T_m). The low-stability mutant V_L-Y49D (annotated with a dashed circle) is arbitrarily assigned a melting temperature of 40 degrees. Color coding follows Figure 1. Distributions of buried surface area of all mutants are shown in **Supplementary Figure 14**.

Interaction between V_L-Y49 and HCDR3 V_H-Y100E is a critical determinant of stability

We examined the anion-π-π interactions between the triplet V_H-D101:V_H-Y100E:V_L-Y49 in all mutants (**Figure 5A, B**). The distances between the alpha carbons of these residues showed that stability-improved mutants (V_H-V102Y, V_H-V102D) mimic those values reminiscent to the WT data

while stability-compromised mutants have disrupted the interactions particularly between V_L-Y49 and V_H-Y100E (**Figure 5C).** The V_L-Y49:V_H-100E interaction is a π-π stacking contact that is located at the HCDR3-LFW2 interface, so we checked whether other interactions on this V_H-V_L interface have a role in this stability loss, but no significant relationship is found (**Supplementary Figures 15, 16)**. This result shows that HCDR3 has a substantial effect on stability, especially through the residue V_H-Y100E. Even the addition of affinity/stability increasing V_H-V102D/Y mutation did not rescue the stability of V_L-Y49N mutant, it got even worse (**Figure 1E**). Therefore, V_L-Y49:V_H-Y100E interaction at the core of the V_H-V_L interface is proven to be very crucial for the overall antibody stability.

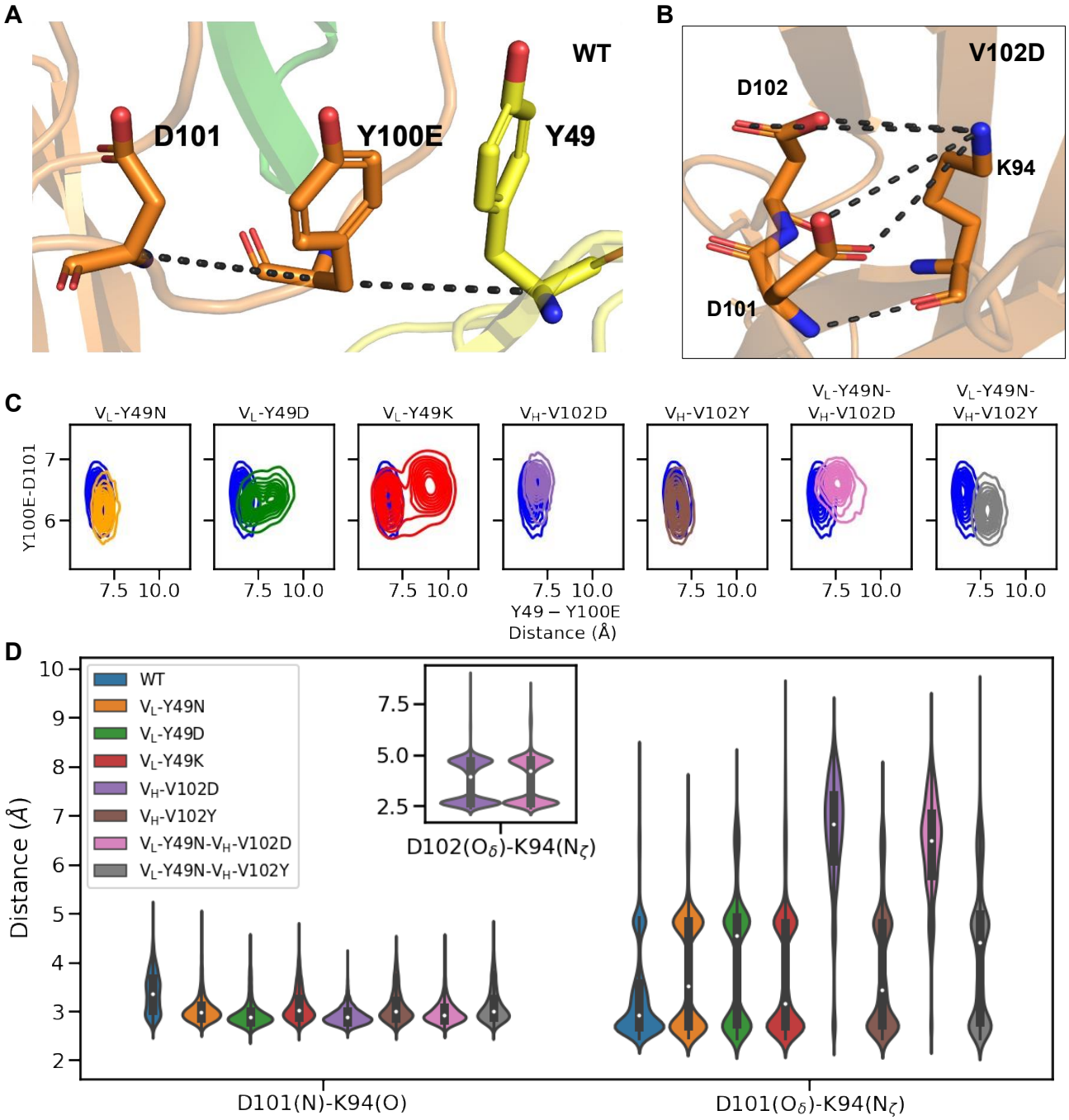

Figure 5: Antibody stability as assessed via critical inter-residue distances at the V_H-V_L interface. **(A)** The anion-π-π interaction (V_H-D101:V_H-Y100E:V_L-Y49) at the V_H-V_L interface of HCDR3-LFW2. (**B)** The core salt bridge V_H-K94:V_H-D101 and the complex salt bridge V_H-K94: V_H-D101/D102 in V_H-V102D **(C)** Distances between the C_α atoms of V_L-Y49:V_H-Y100E and V_H-Y100E:V_H-D101 residues. Distance values of mutants are plotted together with the WT counterpart to demonstrate the shifts. **(D)** Distances between the O atom of V_H-K94 and N atom of V_H-D101 that is the backbone salt bridge and distances between the N_ζ atom of V_H-K94 and O_δ atom of V_H-D101 that is the side-chain salt bridge for all variants. V_H-V102D mutation is also invented a new ionic interaction with its side chain oxygen atom that competes with the ionic interaction of V_H-D101 oxygen atom, shown as an inset. Color coding follows Figure 1.

A *de novo* salt bridge near the stem of HCDR3 leads to a substantial affinity improvement in V102D

While the improvements in stability in the two V_H-V102 mutants can be primarily traced to a more robust HCDR3-V_L interface, affinity improvements occur mainly through the improved HCDR3-VEGF interactions (**Supplementary Figures 10, 11)**. The V_H-V102D forms a complex salt bridge where one residue forms ionic interaction with more than one residue (**Figure 5B**) [48, 71]. The core salt bridge (V_H-K94:V_H-D101) is accompanied by a mutated aspartate (V_H-K94:V_H-D102). Although the backbone ionic interaction of V_H-K94:V_H-D101 is not disrupted at all, side-chain ionic interactions of V_H-K94 were shared with V_H-D101 and V_H-D102 for both V_H-V102D and V_L-Y49N-V_H-V102D mutants (**Figure 5D**). Forming this complex salt bridge between V_H-K94:V_H-D101/D102 might contribute to the affinity increase for both V_H-V102D and V_L-Y49N-V_H-V102D mutants. The indirect effect of V_H-V102 residue on both affinity and stability through HCDR3 loop conformation is notable and worth investigating.

The complex salt bridge at the stem of HCDR3 improves packing of epitope-paratope interaction

When we checked epitope-paratope interactions, VEGF-I91 is found to be the key player by having an interaction with V_H-H101 of HCDR3 (**Supplementary Figure 17)**. We recognized that V_H-H101:VEGF-I91 interaction might explain drastic affinity changes for affinity improved mutants (V_H-V102D, V_H-V102Y, V_L-Y49N-V_H-V102D, V_L-Y49N-V_H-V102Y) by having less distant interaction overall (**Supplementary Figure 17)**. There are also other important epitope-paratope interactions such as V_H-Y102:VEGF-I80, V_H-Y102:VEGF-G92, V_H-G100:VEGF-R82 (HCDR3-VEGF for all), but no significant difference was observed except for double mutants which have the highest improvements in their VEGF affinities that can be attributed to *de novo* contacts formed between side chains and backbone functional groups (**Supplementary Figure 18, 19)**.

To see whether the packing of HCDR3 with VEGF has any contribution to observed affinity, we analyzed the HCDR3 conformation change for V_H-V102D (**Figure 6A**). An angle is calculated to represent tilt of HCDR3 towards VEGF **(Figure 6B).** To measure this angle, two vectors, $\overrightarrow{P_1}$ between the center of masses of scFv and VEGF, $\overrightarrow{P_2}$ between the center of masses scFv and middle residues of HCDR3 (V_H-G100 C_α and V_H-S100A C_α) are used. Θ angle is determined as the cosine angle between those $\overrightarrow{P_1}$ and $\overrightarrow{P_2}$ vectors **(Figure 6B, Supplementary Figure 20)**. Scatter plots of calculated θ angle and experimental affinity change showed that there is an obvious correlation for HCDR3 conformation with affinity changes (**Figure 6C**). While mutants with slight affinity increase (V_L-Y49N, V_L-Y49K, V_H-V102Y) are clustered together with angles values very close to that of WT, mutant with the most significant affinity change (V_H-V102D) had more increase from those of all mutants (**Figure 6C**). This might show that the formation of a complex salt bridge at the stem of HCDR3 might alter overall HCDR3 conformation tilting towards VEGF affecting its affinity drastically.

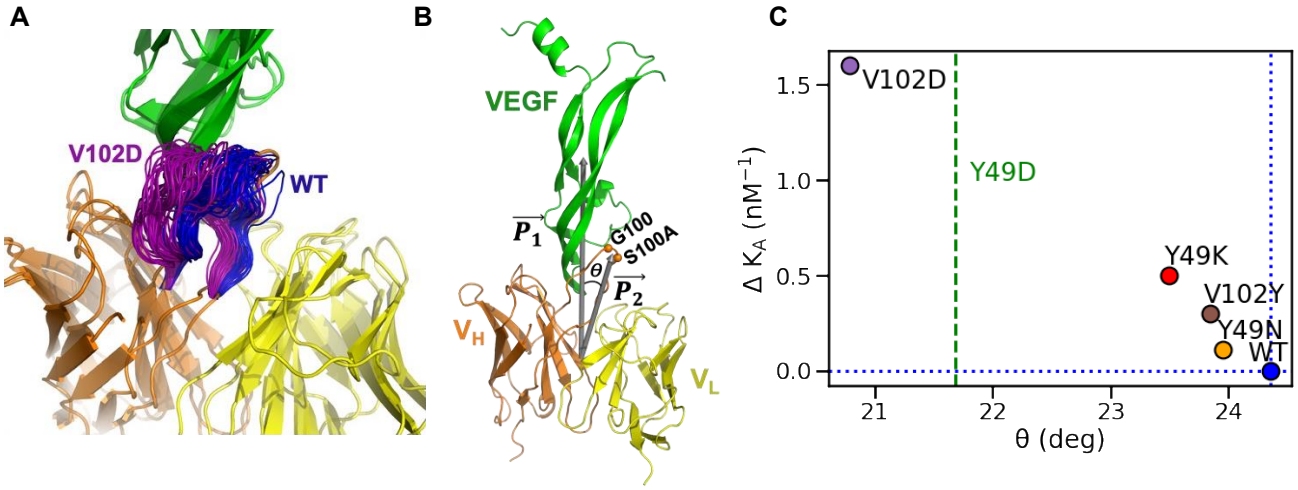

Figure 6: Changes in affinity correlate with a global tilt in HCDR3. **(A)** HCDR3 loop conformations are visualized for WT and V_H-V102D. Alignment is performed based on the reference of the V_H-K94:V_H-D101 salt bridge. HCDR3s are represented as the tubes, HCDR3 frames of V_H-V102D and WT are colored in purple and blue, respectively. **(B)** The cosine angle (θ) change of HCDR3 is calculated between two vectors $\overrightarrow{P_1}$ and $\overrightarrow{P_2}$. $\overrightarrow{P_1}$ vector is the vector between the center of mass of the scFv fragment and the center of mass of antigen VEGF. $\overrightarrow{P_2}$ is the vector between the center of mass of the scFv fragment and the center of masses of V_H-G100 and V_H-S100A C_α atoms. $\overrightarrow{P_1}$ and $\overrightarrow{P_2}$ vectors are colored in gray. Selected atoms are represented as spheres. **(C)** Angle decrease of mutants compared to WT-HCDR3 are scattered through every 100th frame of the whole trajectory (5000 frames). The experimental affinity of the V_L-Y49D mutant could not be obtained, so its representation is made based on our computational results. Color coding follows Figure 1. Distributions of angle of all mutants are shown in **Supplementary Figure 20**.

Discussion

Monoclonal antibodies are promising biomacromolecules for various therapeutic and diagnostic applications. However, numerous trade-offs can be encountered during development and improvement stages due to the intrinsic complexity and the structural limited modularity of these molecules [72]. While the antigen affinity is the most natural and crucial developability parameter, its improvement cannot be decoupled from the stability of the antibody in a systematic manner, resulting in an unavoidable affinity versus stability trade-offs [11, 15, 73]. A primary driver of this mutual dependence could lie in the architecture of the HCDR3 region, an elongated loop that forms critical interactions with both the antigen and the antibody light chain.

In this study, we focused on two pivotal residues (Y49 on the light chain and V102 on the heavy chain) that modulate the global orientation of HCDR3 while maintaining its overall shape and structural integrity (**Figure 1**). Of these two residues, the light chain Y49 tolerated a mutation that improved the antigen affinity but a crucial π-π interaction was lost in the V_H-V_L interface, one that proved irreplaceable for the stability. The second residue of focus, heavy chain V102, not only tolerated mutations that reoriented HCDR3 more favorably for antigen binding, but interactions lost with the light chain could be compensated via novel contacts not present in WT. We identified one such mutation, V_H-V102Y, that demonstrated a joint increase in stability and affinity in both our experimental measurements and atomistic molecular dynamics simulations. HCDR3 has two main interfaces, one toward the antigen and the other one spanning part of the V_H-V_L interface. We have

shown that in these mutants (i) the contacts at the HCDR3-VEGF interface increase, resulting in an improved affinity and (ii) the contacts at the HCDR3, LFW2, and LCDR3 region of the V_H-V_L interface increase, probably resulting in an improved stability. These two mutants are direct evidence that HCDR3 is not only important for affinity but also for stability and not necessarily in an antagonistic manner. We note that caution should be taken to avoid drastic trade-offs during affinity maturation efforts on HCDR3. The findings here are a novel proof of concept demonstration with implications for other antibody engineering efforts.

Understanding antibody stability is a more complex issue because the residues contributing to stability are scattered across diverse positions (core domain, surface exposed residues, V_H-V_L interface) [74-77]. In our study, stability increasing mutations (V_H-V102Y and V_H-V102D) showed significantly higher V_H-V_L interface buried surface area (**Figure 4**). This demonstrates the importance of the scope of V_H-V_L packing for the overall antibody stability. In addition, the V_H-V_L orientation is also known to be important for stability [78-81]. In our mutants, no significant correlation was observed between this metric and stability.

It is known that π-π stacking is very important for protein structure and function. Besides π-π, π-cation/amino/anion contacts are also a part of these crucial stacking interactions [82]. Even triple π-stackings are known to contribute to the activity of proteins [83]. In the specific example of light chain Y49, we mutated this residue to collect structural insights into the effect of triple π-stacking interactions at the V_H-V_L interface. We showed that drastic affinity and stability changes occur when the anion-π-π interaction (V_H-D101: V_H-Y100E:V_L-Y49) was mutated through V_L-Y49N/K/D mutations (**Figure 4, 5**). V_L-Y49 is one of the Vernier zone residues. Although Vernier zone residues are by definition not in the CDR regions (but rather usually at the stem of CDRs), they are known to be indispensable for antibody function [24]. These residues are usually back mutated to restore antibody affinity in humanization efforts [84]. Here, we provide further evidence on the importance of Vernier zone residues for antibody engineering efforts [27].

There is a highly conserved salt bridge (V_H-K94:V_H-D101) at the stem of HCDR3 that is critical for HCDR3 to assume its bulge form [85]. If the lysine (or arginine) at position 94 is converted to any other amino acid, HCDR3 loses function due to lack of stabilizing salt bridge and it does not form the bulge [86]. When this salt bridge was converted into a complex salt bridge by V_H-V102D mutation, affinity and stability increased. In-depth analysis of a molecular dynamics simulation of this mutant showed that the complex salt bridge at the stem shifted the HCDR3 loop to tilt towards VEGF, thereby contributing to the affinity increase (**Figure 6**). Even though V_H-V102 is a highly conserved residue in the antibody framework [87], it is nonetheless a potentially interesting locus for future antibody engineering and affinity maturation efforts. As a general approach, V102 might be mutated to “D” or “Y” to increase antibody affinity with no loss or even better stability. Aspartate in this position is very rare (1%), thus immunogenicity should also be considered while designing mutations with rare amino acids in particular positions.

We should also note here the complementarity aspect of our molecular dynamics simulations in understanding the detailed molecular mechanisms associated with the involvement of HCDR3. Hence all the domains of an antibody share the same structural fold [19, 88] and framework residues, especially chosen HCDR3 salt bridge interaction, are usually very conserved among organisms, these findings can be applied to other antibodies in general. The measured energetic differences in the affinities are on the order of a few thermal energies at ambient conditions (as inferred from the dissociation constants), meaning that accurate prediction of protein-protein binding energies is of utmost importance in this context. As an intuitive measure of the relative changes in binding

interfaces, here, we have used pairwise contacts between the epitope and paratope groups. Such geometric metrics are commonly employed in heuristic correlations with experimentally measured energies [89].

Affinity improvement or re-gaining efforts are usually encountered with numerous trade-offs such as loss of stability, lower solubility, and/or higher aggregation propensity, as reviewed elsewhere [11]. Although these *in vitro* properties of a candidate antibody can be co-screened with a variety of experimental tools, scalability is typically costly and cumbersome. In this context, the use of *in silico* tools can alleviate the load by providing precise predictions at a fraction of the cost and time typically invested in an experimental undertaking. In this work, we tapped into the strength of sufficiently long molecular dynamics simulations which not only validated our physico-chemical wet-lab characterization of our mutants but also provided molecular level understanding into the favorable and unfavorable outcomes.

Acknowledgments

This work was supported by the institutional funds of Izmir Biomedicine and Genome Center (IBG) (T.U., S.Kale, and S.Kalyoncu), Council of Higher Education (YÖK) 100/2000 Fellowship Program (M.A.), The Scientific and Technological Research Council of Turkey (TUBITAK)-BIDEB 2211A PhD Achievement Grant (M.A.), and TUBITAK grant 119Z161 (M.A., S.Kale, and S.Kalyoncu). The authors acknowledge the computational resources of TUBITAK ULAKBIM High Performance and Grid Computing Center (TRUBA resources) and the IBG High Performance Computing Facility.

Conflict of Interest

The authors declare that the research was conducted in the absence of any commercial or financial relationships that could be construed as a potential conflict of interest.

Author Contributions

MA, TU, S.Kale and S.Kalyoncu contributed to conception and design of the study. MA carried out *in vitro* experiments. TU and MA carried out *in silico* analysis. TU and MA performed data visualization. MA and TU wrote the first draft of the manuscript. All authors contributed to manuscript revision, read, and approved the submitted version. S.Kale and S.Kalyoncu supervised the project.

References

1. Kaplon H, Muralidharan M, Schneider Z, Reichert JM. Antibodies to watch in 2020. MAbs. 2020;12(1):1703531.

2. Kaplon H, Reichert JM. Antibodies to watch in 2021. MAbs. 2021;13(1):1860476.

3. Bates A, Power CA. David vs. Goliath: The Structure, Function, and Clinical Prospects of Antibody Fragments. Antibodies (Basel). 2019;8(2).

4. Chao G, Lau WL, Hackel BJ, Sazinsky SL, Lippow SM, Wittrup KD. Isolating and engineering human antibodies using yeast surface display. Nat Protoc. 2006;1(2):755-68.

5. Schofield DJ, Pope AR, Clementel V, Buckell J, Chapple S, Clarke KF, et al. Application of phage display to high throughput antibody generation and characterization. Genome Biol. 2007;8(11):R254.

6. Santos J, Cardoso M, Moreira IS, Goncalves J, Correia JDG, Verde SC, et al. Integrated in Silico and Experimental Approach towards the Design of a Novel Recombinant Protein Containing an Anti-HER2 scFv. Int J Mol Sci. 2021;22(7).

7. Goel A, Colcher D, Baranowska-Kortylewicz J, Augustine S, Booth BJ, Pavlinkova G, et al. Genetically engineered tetravalent single-chain Fv of the pancarcinoma monoclonal antibody CC49: improved biodistribution and potential for therapeutic application. Cancer Res. 2000;60(24):6964-71.

8. Fennell BJ, McDonnell B, Tam AS, Chang L, Steven J, Broadbent ID, et al. CDR-restricted engineering of native human scFvs creates highly stable and soluble bifunctional antibodies for subcutaneous delivery. MAbs. 2013;5(6):882-95.

9. Sawant MS, Streu CN, Wu L, Tessier PM. Toward Drug-Like Multispecific Antibodies by Design. Int J Mol Sci. 2020;21(20).

10. Julian MC, Lee CC, Tiller KE, Rabia LA, Day EK, Schick AJ, 3rd, et al. Co-evolution of affinity and stability of grafted amyloid-motif domain antibodies. Protein Eng Des Sel. 2015;28(10):339-50.

11. Rabia LA, Desai AA, Jhajj HS, Tessier PM. Understanding and overcoming trade-offs between antibody affinity, specificity, stability and solubility. Biochem Eng J. 2018;137:365-74.

12. Houlihan G, Gatti-Lafranconi P, Lowe D, Hollfelder F. Directed evolution of anti-HER2 DARPins by SNAP display reveals stability/function trade-offs in the selection process. Protein Eng Des Sel. 2015;28(9):269-79.

13. Faber MS, Whitehead TA. Data-driven engineering of protein therapeutics. Curr Opin Biotechnol. 2019;60:104-10.

14. Cohen-Khait R, Dym O, Hamer-Rogotner S, Schreiber G. Promiscuous Protein Binding as a Function of Protein Stability. Structure. 2017;25(12):1867-74 e3.

15. Julian MC, Li L, Garde S, Wilen R, Tessier PM. Efficient affinity maturation of antibody variable domains requires co-selection of compensatory mutations to maintain thermodynamic stability. Sci Rep. 2017;7:45259.

16. Koenig P, Lee CV, Walters BT, Janakiraman V, Stinson J, Patapoff TW, et al. Mutational landscape of antibody variable domains reveals a switch modulating the interdomain conformational dynamics and antigen binding. Proc Natl Acad Sci U S A. 2017;114(4):E486-E95.

17. Xu JL, Davis MM. Diversity in the CDR3 region of V(H) is sufficient for most antibody specificities. Immunity. 2000;13(1):37-45.

18. Bostrom J, Lee CV, Haber L, Fuh G. Improving antibody binding affinity and specificity for therapeutic development. Methods Mol Biol. 2009;525:353-76, xiii.

19. Chiu ML, Goulet DR, Teplyakov A, Gilliland GL. Antibody Structure and Function: The Basis for Engineering Therapeutics. Antibodies (Basel). 2019;8(4).

20. Herold EM, John C, Weber B, Kremser S, Eras J, Berner C, et al. Determinants of the assembly and function of antibody variable domains. Sci Rep. 2017;7(1):12276.

21. Zhao J, Nussinov R, Ma B. The Allosteric Effect in Antibody-Antigen Recognition. Methods Mol Biol. 2021;2253:175-83.

22. Makabe K, Nakanishi T, Tsumoto K, Tanaka Y, Kondo H, Umetsu M, et al. Thermodynamic consequences of mutations in vernier zone residues of a humanized anti-human epidermal growth factor receptor murine antibody, 528. J Biol Chem. 2008;283(2):1156-66.

544 23. Riechmann L, Clark M, Waldmann H, Winter G. Reshaping human antibodies for therapy.
545 Nature. 1988;332(6162):323-7.

546 24. Foote J, Winter G. Antibody framework residues affecting the conformation of the
547 hypervariable loops. J Mol Biol. 1992;224(2):487-99.

548 25. Wu H, Nie Y, Huse WD, Watkins JD. Humanization of a murine monoclonal antibody by
549 simultaneous optimization of framework and CDR residues. J Mol Biol. 1999;294(1):151-62.

550 26. Safdari Y, Farajnia S, Asgharzadeh M, Khalili M. Antibody humanization methods - a review
551 and update. Biotechnol Genet Eng Rev. 2013;29:175-86.

552 27. Arslan M, Karadag D, Kalyoncu S. Conformational changes in a Vernier zone region:
553 Implications for antibody dual specificity. Proteins. 2020;88(11):1447-57.

554 28. Arslan M, Karadag D, Kalyoncu S. Protein engineering approaches for antibody fragments:
555 directed evolution and rational design approaches. Turk J Biol. 2019;43(1):1-12.

556 29. Tiller KE, Tessier PM. Advances in Antibody Design. Annu Rev Biomed Eng. 2015;17:191-
557 216.

558 30. Zhao J, Nussinov R, Wu WJ, Ma B. In Silico Methods in Antibody Design. Antibodies
559 (Basel). 2018;7(3).

560 31. Izrailev S, Stepaniants S, Balsera M, Oono Y, Schulten K. Molecular dynamics study of
561 unbinding of the avidin-biotin complex. Biophys J. 1997;72(4):1568-81.

562 32. Dogan D, Arslan M, Ulucay T, Kalyoncu S, Dimitrov S, Kale S. CENP-A Nucleosome is a
563 Sensitive Allosteric Scaffold for DNA and Chromatin Factors. J Mol Biol. 2021;433(6):166789.

564 33. Rocco AG, Mollica L, Ricchiuto P, Baptista AM, Gianazza E, Eberini I. Characterization of
565 the protein unfolding processes induced by urea and temperature. Biophys J. 2008;94(6):2241-51.

566 34. Lindorff-Larsen K, Trbovic N, Maragakis P, Piana S, Shaw DE. Structure and dynamics of an
567 unfolded protein examined by molecular dynamics simulation. J Am Chem Soc. 2012;134(8):3787-
568 91.

569 35. Collu F, Spiga E, Chakroun N, Rezaei H, Fraternali F. Probing the early stages of prion
570 protein (PrP) aggregation with atomistic molecular dynamics simulations. Chem Commun (Camb).
571 2018;54(57):8007-10.

572 36. Fernandez-Quintero ML, Pomarici ND, Math BA, Kroell KB, Waibl F, Bujotzek A, et al.
573 Antibodies exhibit multiple paratope states influencing VH-VL domain orientations. Commun Biol.
574 2020;3(1):589.

575 37. Yamashita T. Toward rational antibody design: recent advancements in molecular dynamics
576 simulations. Int Immunol. 2018;30(4):133-40.

577 38. Cheng X, Wang J, Kang G, Hu M, Yuan B, Zhang Y, et al. Homology Modeling-Based in
578 Silico Affinity Maturation Improves the Affinity of a Nanobody. Int J Mol Sci. 2019;20(17).

579 39. Yang B, Lin SJ, Ren JY, Liu T, Wang YM, Li CM, et al. Molecular Docking and Molecular
580 Dynamics (MD) Simulation of Human Anti-Complement Factor H (CFH) Antibody Ab42 and CFH
581 Polypeptide. Int J Mol Sci. 2019;20(10).

582 40. Yoshida K, Kuroda D, Kiyoshi M, Nakakido M, Nagatoishi S, Soga S, et al. Exploring
583 designability of electrostatic complementarity at an antigen-antibody interface directed by
584 mutagenesis, biophysical analysis, and molecular dynamics simulations. Sci Rep. 2019;9(1):4482.

41. Chiba S, Tanabe A, Nakakido M, Okuno Y, Tsumoto K, Ohta M. Structure-based design and discovery of novel anti-tissue factor antibodies with cooperative double-point mutations, using interaction analysis. Sci Rep. 2020;10(1):17590.

42. Zhang YN, Zhang XQ, Zhang XC, Xu JW, Li LL, Zhu XY, et al. Key Amino Acid Residues Influencing Binding Affinities of Pheromone-Binding Protein from Athetis lepigone to Two Sex Pheromones. J Agric Food Chem. 2020;68(22):6092-103.

43. Fernandez-Quintero ML, Kroell KB, Hofer F, Riccabona JR, Liedl KR. Mutation of Framework Residue H71 Results in Different Antibody Paratope States in Solution. Front Immunol. 2021;12:630034.

44. Musafia B, Buchner V, Arad D. Complex salt bridges in proteins: statistical analysis of structure and function. J Mol Biol. 1995;254(4):761-70.

45. Shirai H, Kidera A, Nakamura H. H3-rules: identification of CDR-H3 structures in antibodies. FEBS Lett. 1999;455(1-2):188-97.

46. Weitzner BD, Dunbrack RL, Jr., Gray JJ. The origin of CDR H3 structural diversity. Structure. 2015;23(2):302-11.

47. Tsumoto K, Ogasahara K, Ueda Y, Watanabe K, Yutani K, Kumagai I. Role of salt bridge formation in antigen-antibody interaction. Entropic contribution to the complex between hen egg white lysozyme and its monoclonal antibody HyHEL10. J Biol Chem. 1996;271(51):32612-6.

48. Presta LG, Chen H, O'Connor SJ, Chisholm V, Meng YG, Krummen L, et al. Humanization of an anti-vascular endothelial growth factor monoclonal antibody for the therapy of solid tumors and other disorders. Cancer Res. 1997;57(20):4593-9.

49. Zirlik K, Duyster J. Anti-Angiogenics: Current Situation and Future Perspectives. Oncol Res Treat. 2018;41(4):166-71.

50. Muller YA, Chen Y, Christinger HW, Li B, Cunningham BC, Lowman HB, et al. VEGF and the Fab fragment of a humanized neutralizing antibody: crystal structure of the complex at 2.4 A resolution and mutational analysis of the interface. Structure. 1998;6(9):1153-67.

51. Hudson PJ, Kortt AA. High avidity scFv multimers; diabodies and triabodies. J Immunol Methods. 1999;231(1-2):177-89.

52. Le Gall F, Kipriyanov SM, Moldenhauer G, Little M. Di-, tri- and tetrameric single chain Fv antibody fragments against human CD19: effect of valency on cell binding. FEBS Lett. 1999;453(1-2):164-8.

53. Arslan M, Karadag M, Onal E, Gelinci E, Cakan-Akdogan G, Kalyoncu S. Effect of non-repetitive linker on in vitro and in vivo properties of an anti-VEGF scFv. Sci Rep. 2022;12(1):5449.

54. Fernandez-Quintero ML, Hoerschinger VJ, Lamp LM, Bujotzek A, Georges G, Liedl KR. VH -VL interdomain dynamics observed by computer simulations and NMR. Proteins. 2020;88(7):830-9.

55. Best RB, Zhu X, Shim J, Lopes PE, Mittal J, Feig M, et al. Optimization of the additive CHARMM all-atom protein force field targeting improved sampling of the backbone phi, psi and side-chain chi(1) and chi(2) dihedral angles. J Chem Theory Comput. 2012;8(9):3257-73.

56. Huang J, Rauscher S, Nawrocki G, Ran T, Feig M, de Groot BL, et al. CHARMM36m: an improved force field for folded and intrinsically disordered proteins. Nat Methods. 2017;14(1):71-3.

57. Izadi S, Anandakrishnan R, Onufriev AV. Building Water Models: A Different Approach. J Phys Chem Lett. 2014;5(21):3863-71.

58. Wu TT, Kabat EA. An analysis of the sequences of the variable regions of Bence Jones proteins and myeloma light chains and their implications for antibody complementarity. J Exp Med. 1970;132(2):211-50.

59. Abhinandan KR, Martin AC. Analysis and improvements to Kabat and structurally correct numbering of antibody variable domains. Mol Immunol. 2008;45(14):3832-9.

60. Dunbar J, Deane CM. ANARCI: antigen receptor numbering and receptor classification. Bioinformatics. 2016;32(2):298-300.

61. Van Der Spoel D, Lindahl E, Hess B, Groenhof G, Mark AE, Berendsen HJ. GROMACS: fast, flexible, and free. J Comput Chem. 2005;26(16):1701-18.

62. Humphrey W, Dalke A, Schulten K. VMD: visual molecular dynamics. J Mol Graph. 1996;14(1):33-8, 27-8.

63. Adamczak R, Porollo A, Meller J. Combining prediction of secondary structure and solvent accessibility in proteins. Proteins. 2005;59(3):467-75.

64. Studier FW. Protein production by auto-induction in high density shaking cultures. Protein Expr Purif. 2005;41(1):207-34.

65. Wilkins MR, Gasteiger E, Bairoch A, Sanchez JC, Williams KL, Appel RD, et al. Protein identification and analysis tools in the ExPASy server. Methods Mol Biol. 1999;112:531-52.

66. Lucas X, Bauza A, Frontera A, Quinonero D. A thorough anion-pi interaction study in biomolecules: on the importance of cooperativity effects. Chem Sci. 2016;7(2):1038-50.

67. D'Angelo S, Ferrara F, Naranjo L, Erasmus MF, Hraber P, Bradbury ARM. Many Routes to an Antibody Heavy-Chain CDR3: Necessary, Yet Insufficient, for Specific Binding. Front Immunol. 2018;9:395.

68. Swindells MB, Porter CT, Couch M, Hurst J, Abhinandan KR, Nielsen JH, et al. abYsis: Integrated Antibody Sequence and Structure-Management, Analysis, and Prediction. J Mol Biol. 2017;429(3):356-64.

69. Tan PH, Sandmaier BM, Stayton PS. Contributions of a highly conserved VH/VL hydrogen bonding interaction to scFv folding stability and refolding efficiency. Biophys J. 1998;75(3):1473-82.

70. Masuda K, Sakamoto K, Kojima M, Aburatani T, Ueda T, Ueda H. The role of interface framework residues in determining antibody V(H)/V(L) interaction strength and antigen-binding affinity. FEBS J. 2006;273(10):2184-94.

71. Gvritishvili AG, Gribenko AV, Makhatadze GI. Cooperativity of complex salt bridges. Protein Sci. 2008;17(7):1285-90.

72. Bigman LS, Levy Y. Proteins: molecules defined by their trade-offs. Curr Opin Struct Biol. 2020;60:50-6.

73. Shehata L, Maurer DP, Wec AZ, Lilov A, Champney E, Sun T, et al. Affinity Maturation Enhances Antibody Specificity but Compromises Conformational Stability. Cell Rep. 2019;28(13):3300-8 e4.

74. Worn A, Pluckthun A. Different equilibrium stability behavior of ScFv fragments: identification, classification, and improvement by protein engineering. Biochemistry. 1999;38(27):8739-50.

667 75. Chang HJ, Jian JW, Hsu HJ, Lee YC, Chen HS, You JJ, et al. Loop-sequence features and
668 stability determinants in antibody variable domains by high-throughput experiments. Structure.
669 2014;22(1):9-21.

670 76. Lehmann A, Wixted JH, Shapovalov MV, Roder H, Dunbrack RL, Jr., Robinson MK.
671 Stability engineering of anti-EGFR scFv antibodies by rational design of a lambda-to-kappa swap of
672 the VL framework using a structure-guided approach. MAbs. 2015;7(6):1058-71.

673 77. Montoliu-Gaya L, Martinez JC, Villegas S. Understanding the contribution of disulfide
674 bridges to the folding and misfolding of an anti-Abeta scFv. Protein Sci. 2017;26(6):1138-49.

675 78. Worn A, Pluckthun A. Mutual stabilization of VL and VH in single-chain antibody
676 fragments, investigated with mutants engineered for stability. Biochemistry. 1998;37(38):13120-7.

677 79. Hsu HJ, Lee KH, Jian JW, Chang HJ, Yu CM, Lee YC, et al. Antibody variable domain
678 interface and framework sequence requirements for stability and function by high-throughput
679 experiments. Structure. 2014;22(1):22-34.

680 80. Tu C, Terraube V, Tam AS, Stochaj W, Fennell BJ, Lin L, et al. A Combination of Structural
681 and Empirical Analyses Delineates the Key Contacts Mediating Stability and Affinity Increases in an
682 Optimized Biotherapeutic Single-chain Fv (scFv). J Biol Chem. 2016;291(3):1267-76.

683 81. Warszawski S, Borenstein Katz A, Lipsh R, Khmelnitsky L, Ben Nissan G, Javitt G, et al.
684 Optimizing antibody affinity and stability by the automated design of the variable light-heavy chain
685 interfaces. PLoS Comput Biol. 2019;15(8):e1007207.

686 82. Dalkas GA, Teheux F, Kwasigroch JM, Rooman M. Cation-pi, amino-pi, pi-pi, and H-bond
687 interactions stabilize antigen-antibody interfaces. Proteins. 2014;82(9):1734-46.

688 83. Klein BJ, Vann KR, Andrews FH, Wang WW, Zhang J, Zhang Y, et al. Structural insights
689 into the pi-pi-pi stacking mechanism and DNA-binding activity of the YEATS domain. Nat
690 Commun. 2018;9(1):4574.

691 84. Haidar JN, Yuan QA, Zeng L, Snavely M, Luna X, Zhang H, et al. A universal combinatorial
692 design of antibody framework to graft distinct CDR sequences: a bioinformatics approach. Proteins.
693 2012;80(3):896-912.

694 85. Decanniere K, Desmyter A, Lauwereys M, Ghahroudi MA, Muyldermans S, Wyns L. A
695 single-domain antibody fragment in complex with RNase A: non-canonical loop structures and
696 nanomolar affinity using two CDR loops. Structure. 1999;7(4):361-70.

697 86. Al-Lazikani B, Lesk AM, Chothia C. Standard conformations for the canonical structures of
698 immunoglobulins. J Mol Biol. 1997;273(4):927-48.

699 87. Wang N, Smith WF, Miller BR, Aivazian D, Lugovskoy AA, Reff ME, et al. Conserved
700 amino acid networks involved in antibody variable domain interactions. Proteins. 2009;76(1):99-114.

701 88. Janeway CA Jr TP, Walport M, et al. The structure of a typical antibody molecule.
702 Immunobiology: The Immune System in Health and Disease 5th edition. New York: Garland
703 Science; 2001.

704 89. Vangone A, Bonvin AM. Contacts-based prediction of binding affinity in protein-protein
705 complexes. Elife. 2015;4:e07454.

706

Engineering of conserved residues near heavy chain complementary determining region 3 (HCDR3) improves both affinity and stability

Merve Arslan [1,2,†], Tuğçe Uluçay [1, †], Seyit Kale [1], Sibel Kalyoncu [1,*]

[1] Izmir Biomedicine and Genome Center, 35340 Balçova, Izmir, Turkey

[2] Izmir International Biomedicine and Genome Institute, Dokuz Eylul University, 35340 Balçova, Izmir, Turkey

[†] The authors wish it to be known that, in their opinion, the first two authors should be regarded as joint First Authors.

*** Corresponding author:**
Sibel Kalyoncu

Izmir Biomedicine and Genome Center, 35340 Balçova, Izmir, Turkey

Email: sibel.kalyoncu@ibg.edu.tr

Phone: +90 232 4126567

Abstract

Affinity and stability are crucial ~~developability~~ parameters in antibody development and engineering approaches. Although ~~a joint~~ improvement in both metrics is desirable, trade-offs are almost ~~always~~ unavoidable. Heavy chain complementarity determining region 3 (HCDR3) is the best-known ~~and most heavily studied~~ region for antibody affinity but its impact on stability is often neglected. Here, we present a mutagenesis study ~~into a selected number~~ of conserved residues near ~~critical for the integrity of~~ HCDR3 to elicit ~~elucidate~~ the role of this region in the affinity-stability trade-off. ~~without directly mutating it.~~ These key residues are positioned around the conserved salt bridge between V_H-K94 and V_H-D101 which is crucial for HCDR3 integrity. We show that the additional salt bridge at the stem of HCDR3 (V_H-K94:V_H-D101:V_H-D102) has an extensive ~~tremendous~~ impact on this loop's conformation, ~~with room for~~ therefore simultaneous improvement in both affinity and stability. We find that the disruption of π-π stacking near HCDR3 (V_H-Y100E:V_L-Y49) ~~critical contact elements~~ at the V_H-V_L interface cause an irrecoverable loss in stability even if it improves the affinity. Molecular simulations of putative rescue mutants exhibit complex and often non-additive effects. We confirm that our experimental measurements agree with the molecular dynamics simulations providing detailed insights for the spatial orientation of HCDR3. ~~This study shows the power of molecular dynamics studies in complementing our rational antibody design efforts with critical insights from a structural point of view.~~ V_H-V102 right next to HCDR3 salt bridge might be an ideal candidate to overcome affinity-stability trade-off.

Keywords: Antibody, Antibody Engineering, Vernier Zone, Affinity-Stability trade-offs, Molecular Dynamics

Introduction

Antibodies are ~~naturally occurring biological molecules that are~~ widely utilized as diagnostics and therapeutics tools thanks to their high affinity and specificity toward target antigens. Hundreds of therapeutic antibodies in different formats such as Fab, single-chain variable fragment (scFv), or nanobodies, continue being developed and tested in clinical trials [1, 2]. Due to their small size, monovalent nature, and simpler folding paths [3] , scFvs offer several beneficial attributes for *in silico* and *in vitro* developability applications [4-6] . Although scFvs might show some drawbacks such as lower stability, and fast clearance, they are readily suitable for protein engineering strategies to overcome them [7, 8] .The ~~success of these efforts and the~~ eventual success of the antibody depend strongly on its developability properties such as activity and stability. The activity of an antibody is related to its strong and specific binding to its cognate antigen, a metric that is ~~more commonly~~ known as *antigen affinity* [9]. A molecular-level understanding of the ~~this~~ affinity is ~~a~~ challenging, ~~and open question~~ that might limit antibody development. ~~because~~ Affinity improvement efforts can result in detrimental effects on the overall profile [10, 11]. The primary bottleneck here is *stability* which is another important developability parameter often negatively correlated with the ~~antigen~~ affinity [12-14]. For a successful antibody, it is critical to maintaining a necessary level of stability while engineering the affinity. Thus, co-screening of stability and affinity is essential to find the optimal mutations [15, 16].

Affinity modulation efforts have historically focused on the complementarity determining regions (CDRs), particularly heavy chain CDR3 (HCDR3) [17, 18]. These regions are intrinsically *hypervariable* originating from somatic hypermutations in mature B cells which leads ~~leading~~ to CDR sequence diversity [19]. Several studies point out that non-CDR regions (known as framework residues) can also be important for affinity because they impact the overall antibody structure [11, 20, 21]. Affinity gains by

substitutions of non-CDR residues have been generally underestimated in directed evolution strategies. And there has been little systematic study to assess the consequences of this bias. In this context, one of the non-CDR regions ~~that can lead to drastic differences~~ is the Vernier zone [22]. The Vernier zone of an antibody is characterized by a set of critical framework residues underlying the CDRs [23, 24]. These residues potentially affect the conformations of the CDR loops and their orientation with respect to the antigen epitope; thus, they are common targets of humanization efforts to regain affinity via back mutations [22, 25, 26]. Roles of the Vernier zone region on other antibody properties such as specificity and stability remain to be elucidated [27].

Powerful experimental technologies such as directed evolution and rational designs have made *in vitro* evolution of antibodies ~~progressively~~ more efficient and have taken the field of modern antibody engineering further [28]. While experimental approaches can generally provide reliable results, scalability can be cumbersome, labor-intensive, and prohibitively expensive [29]. In this context, *in silico* approaches can provide invaluable opportunities with their high-throughput potential and ready access to atomic-level details [30]. Molecular dynamics (MD) simulations investigate the biomolecular structures of antibodies at their natural dynamics on timescales relevant to their physiological function. These efforts can provide critical supporting information, including (i) computed free energy differences and measured forces behind protein-protein binding [31, 32], (ii) atomic-level dynamics, (iii) information about protein stability in different physiological and experimental conditions [33-35] and (iv) the nature of the interactions between an antibody and its cognate antigen [36]. MD methods combined with rational design approaches can be used to design better antibodies in a shorter time, with improved accuracy and at a reduced cost [37]. The number of successful examples of this approach published in literature is on the rise [38-43].

In this study, we generated rationally chosen mutations on an anti-Vascular Endothelial Growth Factor (VEGF) scFv to investigate their effects on affinity and stability. Salt bridges are one of the most critical non-covalent forces in protein structure and function [44]. The salt bridge between the two heavy-chain residues 94 and 101 (according to Kabat numbering) is a highly conserved structural motif that supports the robust shape of HCDR3 [45, 46]. Modifying or altering this interaction is virtually always detrimental for both stability and affinity [47]. Motivated by this critical observation, we hypothesized that the vicinity of this salt bridge is a natural starting point to investigate the trade-off between affinity and stability. To this end, we generated an anti-VEGF scFv antibody [48] and designed mutations in both heavy chain (V_H) and light chain (V_L) sides of this salt bridge accompanying the Vernier zone residues around (**Figure 1A**). Anti-VEGF antibodies are successful anti-cancer therapeutics [49] and thanks to its universal nature of the Vernier zone, the lessons learned in this study could be transferable to other antibodies in general. We performed both comparative molecular dynamics simulations and experimental characterizations to gain a molecular-level understanding of the factors that modulate this trade-off. We found that existing and *de novo* secondary/tertiary interactions around this HCDR3 salt bridge are a critical determinant of both antigen binding and the robustness of the V_H-V_L interface, thus playing a crucial and complex role in the co-evolution of affinity-stability. Our overall findings obtained from our experimental and MD studies show the importance of joint efforts to elucidate the molecular mechanisms of antibody design.

Materials and Methods

Setup Preparation and analysis of Molecular Dynamics Simulations

Atomic coordinates of the anti-VEGF scFv antibody fragment were taken from the Protein Data Bank (PDB ID:1BJ1; chains H, L and W) [50]. Constant fragment groups and the linker between the variable groups were omitted. When scFv linker length is longer than 12 residues, covalently linked V_H and V_L form a functional and monomeric scFv [51-53] and it was previously shown that absence of linker do not affect calculated distributions of molecular dynamic simulations [54]. Amino acid distributions of each Kabat numbering positions were extracted from AbYsis database (www.abysis.org). Mutant constructs were prepared using the Wizard Mutagenesis tool of PyMOL Molecular Graphics System, version 2.1.1, Schrödinger LLC. Each antibody-antigen complex is solvated in a cubic water box that is sufficiently large to provide a minimum buffer zone of 12 Å between biological material and the cubic system boundaries. Na^+ and Cl^- ions were placed randomly to neutralize the system electrostatically at a physiological salt concentration of 0.150 M. CHARMM36m force field [55, 56] was chosen together with the four-site OPC water model [57] subject to periodic boundary conditions. A combination of conjugate gradient and steepest descent methods were applied for initial energy minimization. Later, the system was equilibrated in the NVT ensemble at 100K for 1 ns, and at 310K for 1 ns, both using a small integration time step of 1 fs. Production trajectories were collected in the NPT ensemble at 310K and 1 atm atmospheric pressure using a 2 fs of integration time steps for a total of 500 ns. Atomic coordinates were saved every 100 ps.

Kabat numbering scheme and the domain definitions were used to determine complementarity-determining regions (CDRs) and the frameworks (FWs) [58, 59] utilizing the web server SabPred-Anarci [60]. Since there are some differences between the Kabat number of the residues and the deposited structure number of the residues, the alignments of the numbering schemes were presented in **Supplementary Figure 1.** The contacts and distances between V_H and V_L chains were utilized to assess stabilities, the contacts and distance between both antibody chains and the antigen for affinities. A contact between two interacting domains was defined geometrically for when two heavy (i.e., non-hydrogen) atoms are close to each other within a cutoff of 5 Å or less. Contacts were averaged over all recorded molecular configurations in each trajectory (5000 frames for each simulation). The proximity between two given residues was calculated by the distance between the centers of mass of interacting atoms of given residues. Root mean square fluctuations (RMSFs) were calculated based on the α-carbons of protein chains. The area of the V_H-V_L interface is calculated by subtracting the solvent-accessible surface area (SASA) of the complexed V_H-V_L pair from the sum of the SASAs of the individual V_H and V_L domains. Mass centers, per residue RMSFs, SASA computations were performed by VMD-Python library (https://vmd.robinbetz.com/), and distances between the centers were computed by Python's Numpy. Gromacs version 2018.3 [61] was used for all simulation setups and for the collection of trajectories. VMD [62] and in-house Python scripts were used for all analyses and visualizations.

In silico secondary structure prediction

The secondary structure of the wild-type and all mutant antibodies were predicted via SABLE prediction webserver [63]. One letter amino acid codes of the antibody sequences were used as input separately. Secondary structure was chosen for prediction goal, SABLE II was chosen for server version, WApproximator was chosen for predictor type.

Protein constructs and protein expression

The anti-VEGF single chain antibody fragment (scFv) heavy chain (V_H) and light chain (V_L) fused via a 21 amino acids length non-repetitive linker "SPNSASHSGSAPQTSSAPGSQ" [53]. The scFv mutants were generated by QuikChange Lightning Site-Directed Mutagenesis Kit (Agilent). The

scFv mutants with the leader sequence (PelB), FLAG-tag and polyhistidine-tag were transformed into *E.coli* strain BL21 (DE3) pLysS (Thermo Fisher) with pET17-b (GenScript) expression plasmid. Transformant cells were grown on LB-agar plates containing 100µg/mL ampicillin and 25µg/mL chloramphenicol. Single colonies were inoculated in LB broth containing 100µg/mL ampicillin and 25µg/mL chloramphenicol and grown overnight at 225 rpm, 37 °C. These cells were inoculated into 300 mL autoinduction-media and incubated at 18°C, 250 rpm for 48 h [64].

Protein purification

Cultures were centrifuged at 6500xg and 4°C (Avanti, Beckman Coulter). Protein containing supernatant was incubated with His-Pur Ni-NTA resin (Thermo Fisher) for 2 h at 4°C shaking vigorously. The mixture was loaded into a 10 ml vacuum column (Thermo Fisher) and purified according to recommended commercial protocol. Phosphate buffered saline (PBS) with 25 mM Imidazole, pH 7.4 and PBS with 500 mM Imidazole, pH 7.4 were used as wash and elution buffers, respectively. Purified protein was buffer-exchanged into PBS (pH 7.4) through membrane filtration (Amicon® Ultra-4 Centrifugal Filter Units, MWCO 10 kDa, Merck). Protein samples were loaded onto HiTrap ™ Protein L column (GE Healthcare) as a second purification step to maximize protein purity. Protein purities were confirmed on sodium dodecyl sulfate-polyacrylamide gel electrophoresis analysis (TGX ™, FastCast™, 12% Acrylamide kit; Bio-Rad). Precision Plus Protein™ Dual Color standard was used as a marker (Bio-Rad). Protein concentrations were determined by NanoDrop 2000 (at 280 nm). Extinction coefficients were determined 68550 M^{-1} cm^{-1} for WT and V_H-V102D, 67060 M^{-1} cm^{-1} for V_L-Y49D, V_L-Y49K, V_L-Y49N, 70040 M^{-1} cm^{-1} for V_H-V102Y via Expasy ProtParam webserver while using the protein sequences as input [65].

Thermal denaturation assay

Thermal unfolding profiles of purified scFv proteins were determined by thermal shift assay by ABI 7500 Fast RT-PCR. SYPRO™ Orange Protein Gel Stain (Thermo Fisher) at 5x concentration was used with a 5 µM antibody concentration. Temperature range of 25-99°C with a 0.05% ramp rate was used. Thermal transition mid-points (i.e., T_m values) from the thermogram data were determined using the Hill equation fit by Origin 8.5 software.

Surface Plasmon Resonance (SPR)

Affinity measurements were performed using surface plasmon resonance (SPR) on a Biacore T200 instrument (Biacore Inc., Piscataway, NJ). All experiments were performed in an HBS-EP buffer, pH 7.4. 1000 nM His-tagged VEGF protein was immobilized on a CM4 chip at a flow rate of 10 µl/min for ~1 min (target RU for immobilization was 100 RU). A series of solutions ranging from 10 to 100 nM scFv fragments were subsequently injected at a flow rate of 30 µl/min onto the VEGF-immobilized surface. Regeneration was performed with 10 mM glycine-HCl at pH 2.7 at a flow rate of 30 µl/min for 30 seconds after each concentration in the run. Data were corrected by double-referencing against a control flow cell containing no VEGF and injecting buffer solution. Sensogram curves were analyzed using the BiaEval 3.0 manufacturer's software. K_D, k_{on} and k_{off} values were calculated by fitting the kinetic association and dissociation curves to a 1:1 binding model.

Results

Rationale behind mutational designs

Two positions, one from light chain (V_L-Y49) and one from heavy chain (V_H-V102) are chosen to evaluate affinity/stability trade-offs through secondary interactions of the conserved salt bridge (V_H-K94 and V_H-D101) under the stem of HCDR3. V_L-Y49 is a conserved framework residue which is positioned at the V_L-HCDR3 interface. ~~This tyrosine~~ V_L-Y49 makes π-π contacts with an HCDR3 residue, V_H-Y100E. On the other hand, V_H-Y100E makes an either hydrophobic or anion-π contact with V_H-D101 [66], so there is an anion-π-π interaction between those three residues (V_H-D101:V_H-Y100E:V_L-Y49, **Figure 1A**). For V_L-Y49, we designed three mutations, Y49N to evaluate anion-π-amino interaction, Y49K to evaluate anion-π-cation interaction and Y49D, anion-π-anion interaction. Because this position is surface accessible, all these mutations would also help to improve solubility leading to a possible stability increase. However, Y49D mutation is designed as disruptive mutation due to possibility of repulse between two negatively charged amino acids, V_L-D49:V_H-D101.

V_H-V102 is the last residue of HCDR3, does not have contacts with antigen and it is relatively conserved according to its distribution in *Homo sapiens* (**Supplementary Figure 5). ~~4)~~.** The most common residue is tyrosine (33%) followed by valine (24%). This residue is also highlighted as one of the key stabilizing contacts for HCDR3 structural diversity [46]. On the other hand, aspartate in this position is rarely found (1%). We designed two mutations for this position: V_H-V102Y and V_H-V102D. While V_H-V102Y would show the difference between the two most conserved amino acids, V_H-V102D might form complex salt bridge at the stem of HCDR3 and it might also improve stability in soluble conditions due to its negative charge.

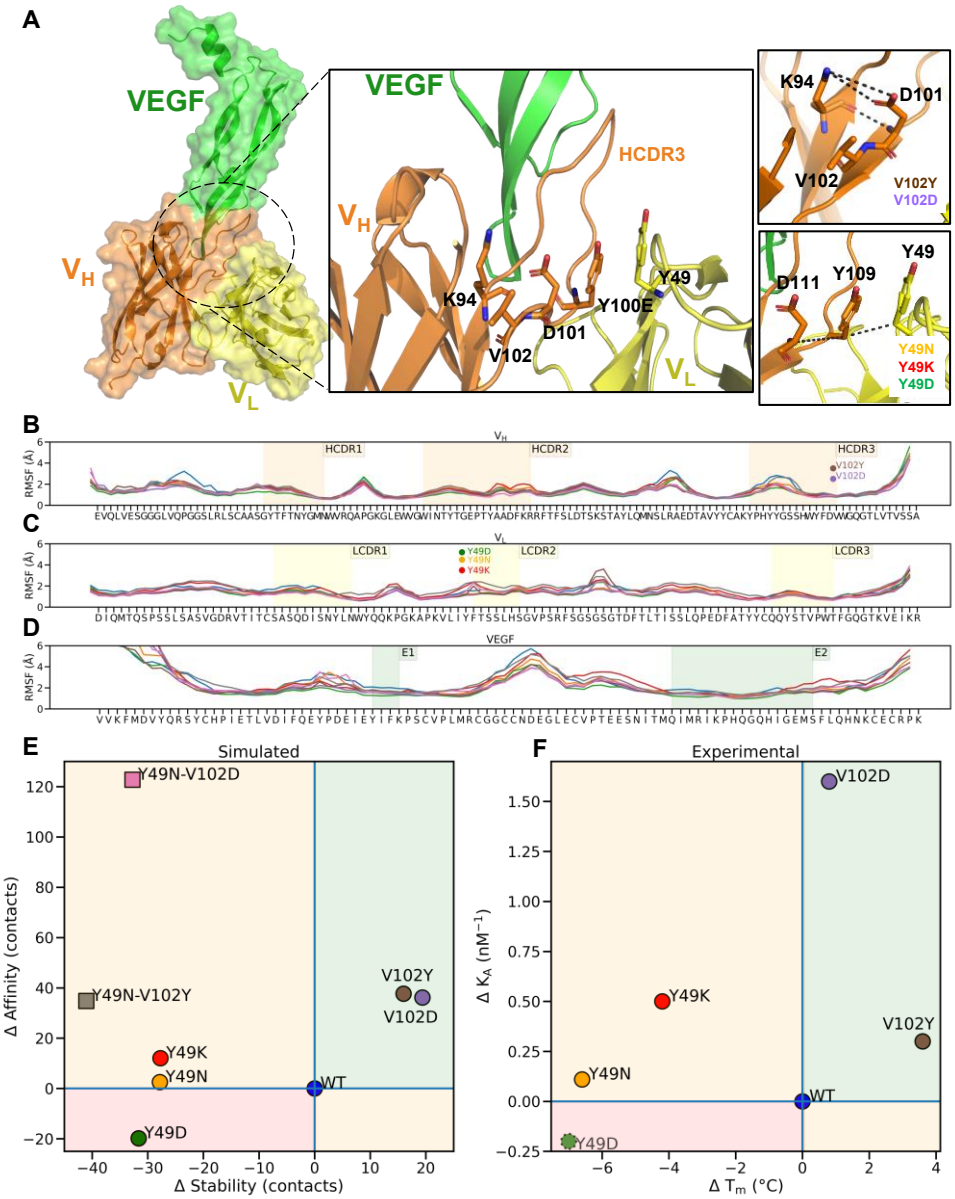

Figure 1: Mutations in the vicinity of the conserved salt bridge (V_H-K94:V_H-D101) of the variable heavy chain modulate antibody affinity and stability characteristics. **(A)** View of the antigen (Vascular Endothelial Growth Factor, VEGF) bound to its cognate scFv fragment (left panel, PBD

ID: 1BJ1 [50]). Insets show the salt bridge as well as the nearby mutational landscape investigated in this study (center and right panels, respectively). Orange, yellow, and green colors indicate the scFv heavy chain (V_H), scFv light chain (V_L) and VEGF proteins, respectively. The conserved salt bridge between V_H residues K94 and D101 is indicated via dashed black lines (top right panel). Rational mutations on scFv involve residues V102 (on V_H) and Y49 (on V_L). **(B-D)** Molecular dynamics of the wild-type (WT) and mutated scFv constructs. The flexibility of the proteins are illustrated by the average root mean square fluctuations (RMSFs) of backbone atoms of the heavy chain **(B)**, the light chain **(C)** and the antigen VEGF **(D)**. Blue, orange, red, green, brown, purple, pink and gray lines indicate WT, V_L-Y49N, V_L-Y49K, V_L-Y49D, V_H-V102Y, V_H-V102D, V_L-Y49N-V_H-V102D, V_L-Y49N-V_H-V102Y mutants, respectively. This color convention is used throughout the rest of the text. Complementarity determining regions (CDRs) of the heavy chain, the light chain and the epitopes of VEGF are highlighted in orange, yellow and green, respectively. Mutated residues are annotated with circles. The time evolution of the V_H:V_L contacts for all mutants are shown in **Supplementary Figure 2 ~~1~~.** The time evolution of the antibody:antigen contacts for all mutants are shown in **Supplementary Figure 3 ~~2~~. (E-F)** Scatter plots of affinity and stability differentials with respect to the WT antibody. The green areas represent "increased affinity and increased stability", red "decreased affinity and decreased stability" and oranges "decreased affinity or stability", meaning a trade-off. **(E)** Computed contact differentials from the molecular dynamics trajectories (See Methods). Differences in the mean of total contact counts between the V_H and V_L chains (an indicator of stability, x-axis) and between scFv and VEGF (an indicator of affinity, y-axis) with respect to their WT counterparts are shown. Distribution of contact counts between VH:VL (stability) and antibody antigen (affinity) are shown in **Supplementary Figure 4A ~~3A~~ and 4B ~~3B~~**, respectively. **(F)** Experimentally measured stability (T_m, thermal melting temperature, x-axis) and affinity (as illustrated via $K_A = 1/K_D$, the association constant, y-axis) differentials of each mutant with respect to the WT. The experimentally unstable construct V_L -Y49D is annotated via a dashed-edged circle. Considering ~~In light of~~ their discouraging MD properties, we did not attempt to produce the two double mutants (V_L-Y49N-V_H-V102D, V_L-Y49N-V_H-V102Y) (square marks in **E**).

Affinity and stability profiles of designed scFvs

The conserved salt bridge between V_H-K94:V_H-D101 at the stem of HCDR3 defines the robustness of this loop **(Supplementary Figure 5). ~~4).~~** HCDR3 is the main paratope for most antigens [67], thus we designed several mutations around this salt bridge, preferentially on a Vernier zone residue. We aimed to modulate the antigen affinity without compromising HCDR3 because it is critical that the stem of HCDR3 has a light-chain interface that can contribute to the stability of the antibody. We chose residues V_H-V102 and V_L-Y49 to understand the secondary/tertiary effects on the V_H-V_L interface (**Figure 1A**). In the MD simulations of these constructs, average root means square fluctuations (RMSF) values near the mutations remained within the range of 6 to 10 Å, indicating that the antibody and antigen structures can still maintain a robust binding configuration. These results suggest that the overall structural flexibility of scFvs is not altered significantly by the introduced mutations **(Figure 1B-D)**. *In silico* secondary structure predictions also showed that point mutations are well tolerated within scFv secondary structure **(Supplementary Figure 6).** However, the conserved or drastic mutations on V_H-V102 and V_L-Y49 revealed notable affinity and/or stability changes [68] (**Figure 1B-F, Figure 2**).

On the V_H side, while V_H-V102Y is a mutation to a more conserved residue for this specific position (33% Y, 24% V, **Supplementary Figure 5), ~~4),~~** V_H-V102D mutation is a drastic change to see whether the ionic bonding of the salt bridge at the stem of HCDR3 is disrupted by the introduction of a proximal acidic residue. Both mutations improve affinity and stability as suggested jointly by our

MD simulations and experimental measurements (**Figure 1E, F, Figure 2**). Only V102D has a higher than predicted affinity while showing slight difference in stability.

HCDR3 is in direct contact with the V_L chain through the V_H-Y100E:V_L-Y49 π-π interaction (**Figure 1A**). Although V_H-Y100E is in HCDR3, this π-π stacking proves to be a crucial contact for the V_H-V_L interface and the HCDR3 robustness through V_H-D101:V_H-Y100E:V_L-Y49 anion-π-π stacking. We designed V_L-Y49K, V_L-Y49N and V_L-Y49D mutations to convert this triple stacking into anion-π-cation, anion-π-amino and anion-π-anion, respectively. Here, we designed the V_L-Y49D mutant as a negative control to disrupt this stacking interaction and we showed that it has very low stability according to MD simulations. Probably related to this stability loss, it even could not be ~~experimentally~~ recombinantly produced (**Figure 1E, F**). The other mutants were successfully produced and purified from the supernatant (**Figure 2A**). Among the mutants, V_H-V102Y showed the highest increase in thermal stability while V_H-V102D mutant improved the thermal stability slightly compared to WT (**Figure 2C**). Those two mutants also showed improved affinity in SPR analysis (**Figure 2B, Supplementary Figure 7).** ~~5).~~ Although V_L-Y49N, V_L-Y49K mutations showed slightly increased affinity, their stability is compromised according to both computational and experimental findings (**Figure 1B-F, Figure 2B-C, Supplementary Figure 7).** ~~5).~~

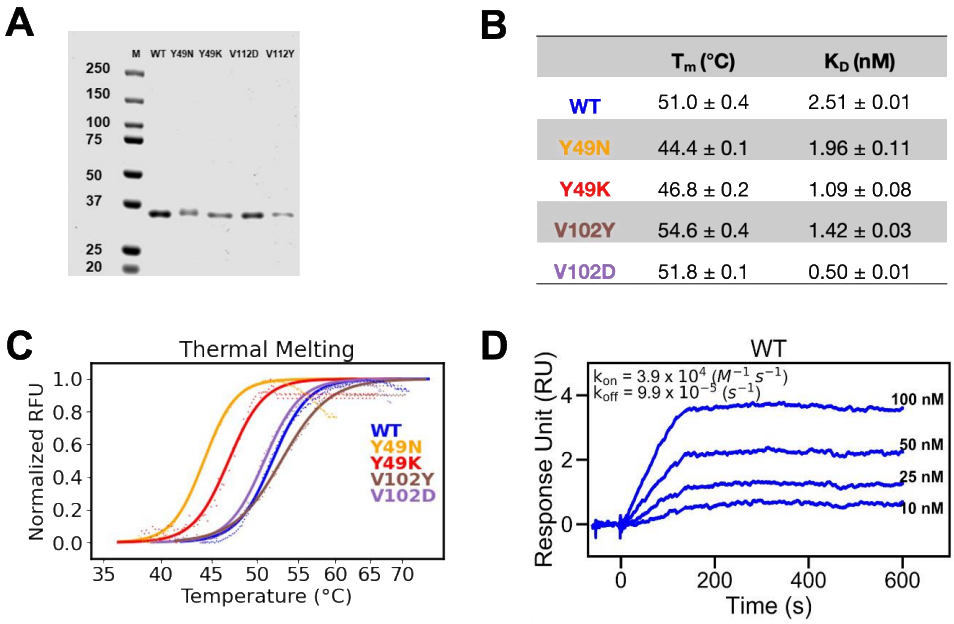

	T_m (°C)	K_D (nM)
WT	51.0 ± 0.4	2.51 ± 0.01
Y49N	44.4 ± 0.1	1.96 ± 0.11
Y49K	46.8 ± 0.2	1.09 ± 0.08
V102Y	54.6 ± 0.4	1.42 ± 0.03
V102D	51.8 ± 0.1	0.50 ± 0.01

Figure 2. Experimental affinity and stability profiles of scFv constructs in this study. **(A)** SDS-PAGE analysis of scFvs after bacterial expression and purification, **(B)** Thermal melting temperature (T_m, in degrees) and dissociation constant (K_D, in molarity units) values, **(C)** T_m plots (repeated at least two times in three replicates with different batches of protein) **(D)** SPR profile of WT for affinity determination (SPR profiles of all mutants are in **Supplementary Figure 7).** ~~5).~~Color coding follows Figure 1.

Rescue mutations have non-additive effects

To restore the stability loss of V_L-Y49N by the stability-favoring mutations (V_H-V102D and V_H-V102Y), we designed two *in silico* double mutants, V_L-Y49N:V_H-V102D and V_L-Y49N:V_H-V102Y. Surprisingly, both rescue mutants showed even worse stability profiles as observed in the MD simulations (**Figure 1E**). As a result, we did not pursue these mutants experimentally. Most importantly, this finding shows that the effects of single point mutations are not additive and more complex secondary/tertiary interactions are at play for affinity/stability profiles. We tried to have an insight into the affinity/stability profiles of our designed mutants through more detailed structural studies.

HCDR3 is essential for both affinity and stability

Computed pairwise contact counts between the protein components of V_L-Y49N suggested specific regions for the increase in affinity and the loss in stability (**Figure 3**). While the affinity gain is mostly due to HCDR3-VEGF contact increase as expected, stability decrease is mostly caused by V_H-V_L interface disruption through HCDR3, LCDR3 and/or light framework 2 (LFW2) contact loss (**Figure 3A, B**). As expected, VEGF binding occurs mostly with V_H chain (**Figure 3C**). Same regions (HCDR3-VEGF for affinity, HCDR3, LCDR3 and LFW2 for stability) play similar roles in other mutants **(Supplementary Figures 8-13)**. ~~**6-11).**~~ Although V_H-V102Y and V_H-V102D mutants are not directly in the V_H-V_L interface, they have a drastic stability increase probably due to secondary HCDR3 interactions and/or stronger intra-HCDR3 contacts. We can examine the HCDR3 loop on two sides, one face to VEGF (HCDR3 residues 95-100B) that play roles in binding and shows mostly change in VEGF binding, while the other face (HCDR3 residues 100B-102) shows changes in V_L interacting surface (**Figure 1A**). This emphasizes that HCDR3 has crucial roles in both affinity and stability profiles of antibodies.

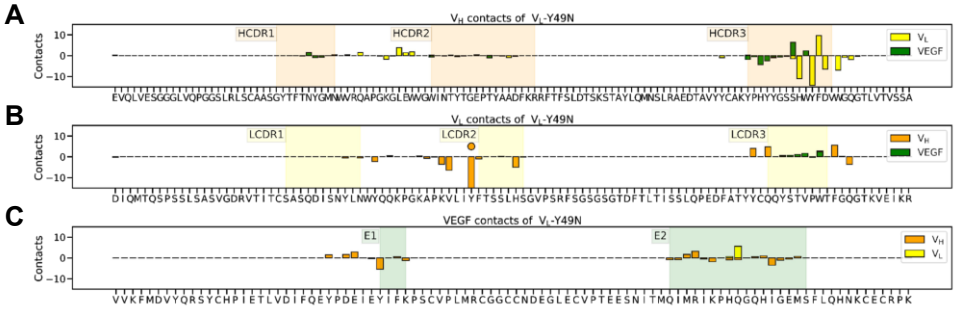

Figure 3. Difference in pairwise contact counts of V_L-Y49N mutant with respect to WT. V_H, V_L and VEGF interactions per residue are colored orange, yellow and green, respectively. **(A)** V_L and VEGF contact count differences for V_H residues. **(B)** V_H and VEGF contact count differences for V_L residues. Mutated residue is annotated with a circle. **(C)** V_H and V_L contact count differences for VEGF residues. FW regions are not shown: FW1 is before CDR1, FW2 is in between CDR1-CDR2, FW3 is in between CDR2-CDR3, FW4 is in after CDR3. Color coding follows Figure 1.

V_H-V_L interface is compromised in low-stability mutants

The V_H-V_L interface and its packing are known to have a significant effect on the stability of an antibody [69, 70]. We analyzed the V_H-V_L interface by computing the buried surface areas (BSAs) of each mutant (**Figure 4, Supplementary Figure 14)**. ~~12).~~ We calculated this property by subtracting solvent accessible surface area (SASA) of the complete V_H-V_L complexes from the sum of the SASAs of the individual V_H/V_L proteins (**Figure 4A**). Mutants with high measured thermal melting points (V_H-V102Y, V_H-V102D) also have computed BSA values close to or higher than that of the WT (~1750 $Å^2$ or higher). On the other hand, mutants with low measured thermal melting points (V_L-Y49N, V_L-Y49K, V_L-Y49D) also have computed BSA values that are less than of that of the WT (lower than 1700 $Å^2$, **Figure 4B**).

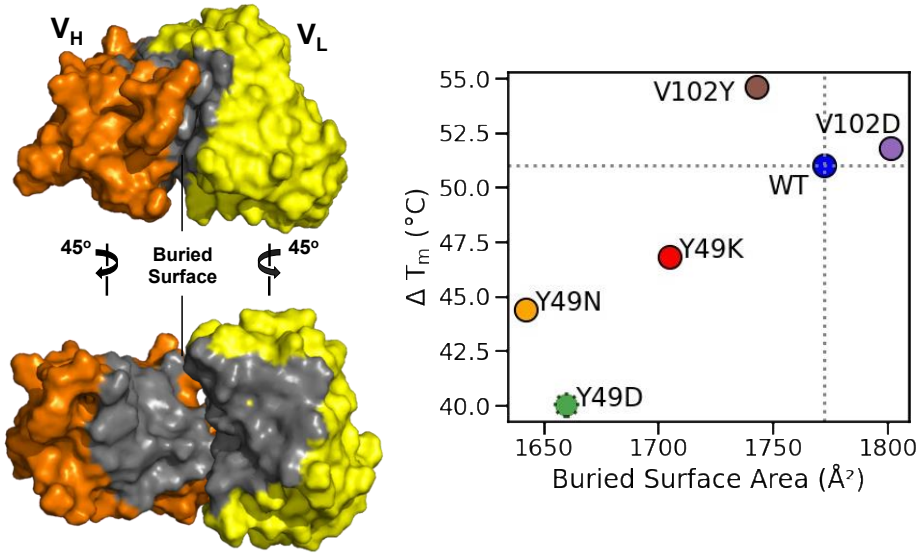

Figure 4: Correlation between measured thermal stabilities and computed V_H-V_L buried surface areas of all mutants. The area of the V_H-V_L interface is calculated by subtracting the solvent-accessible surface area (SASA) of the complexed V_H-V_L pair from the sum of the SASAs of the individual V_H and V_L domains. **(A)** Surface representation of the calculated buried surface area. Surfaces of V_H, V_L and their buried surface areas are colored orange, yellow and gray, respectively. **(B)** Computed average buried surface areas are scattered with the experimental melting temperature values (T_m). The low-stability mutant V_L-Y49D (annotated with a dashed circle) is arbitrarily assigned a melting temperature of 40 degrees. Color coding follows Figure 1. Distributions of buried surface area of all mutants are shown in **Supplementary Figure 14.** ~~12.~~

Interaction between V_L-Y49 and HCDR3 V_H-Y100E is a critical determinant of stability

We examined the anion-π-π interactions between the triplet V_H-D101:V_H-Y100E:V_L-Y49 in all mutants (**Figure 5A, B**). The distances between the alpha carbons of these residues showed that stability-improved mutants (V_H-V102Y, V_H-V102D) mimic those values reminiscent to the WT data

while stability-compromised mutants have disrupted the interactions particularly between V_L-Y49 and V_H-Y100E (**Figure 5C).** The V_L-Y49:V_H-100E interaction is a π-π stacking contact that is located at the HCDR3-LFW2 interface, so we checked whether other interactions on this V_H-V_L interface have a role in this stability loss, but no significant relationship is found **(Supplementary Figures 15, 16)**. ~~**13, 14).**~~ This result shows that HCDR3 has a substantial effect on stability, especially through the residue V_H-Y100E. Even the addition of affinity/stability increasing V_H-V102D/Y mutation did not rescue the stability of V_L-Y49N mutant, it got even worse (**Figure 1E**). Therefore, V_L-Y49:V_H-Y100E interaction at the core of the V_H-V_L interface is proven to be very crucial for the overall antibody stability.

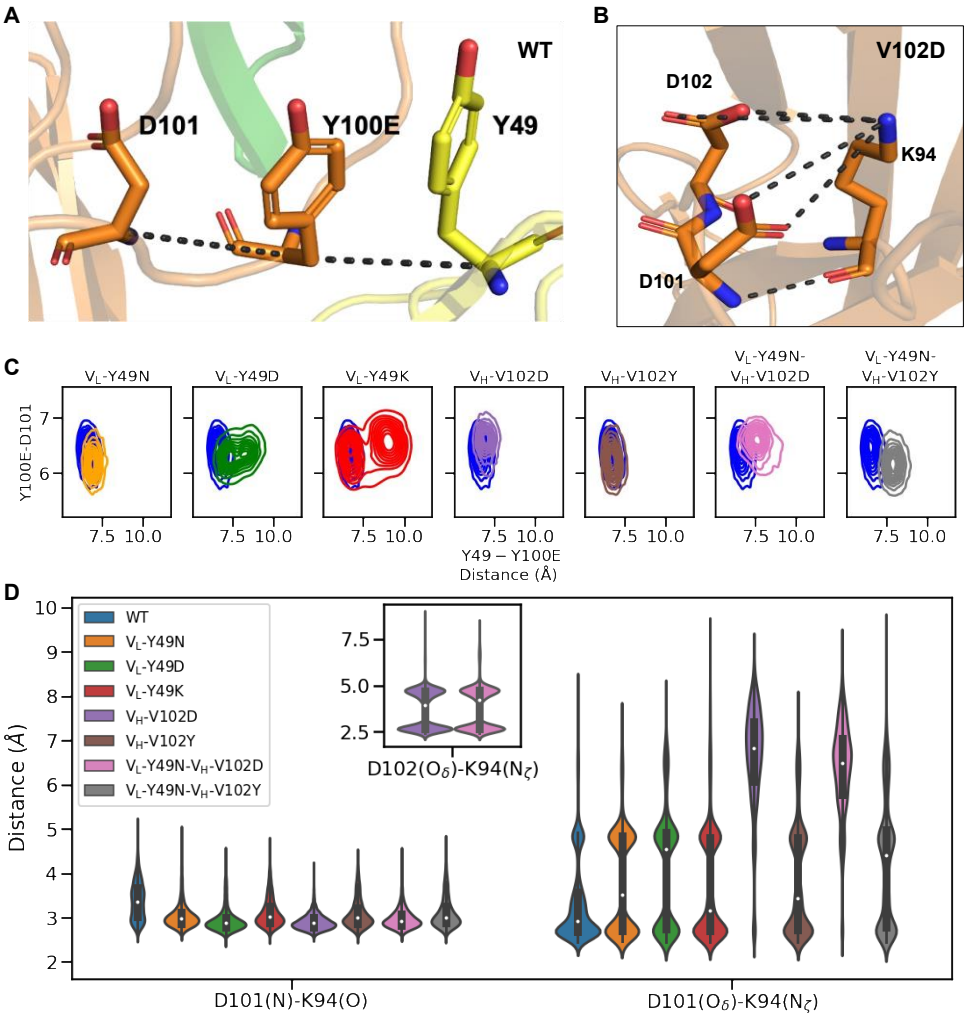

Figure 5: Antibody stability as assessed via critical inter-residue distances at the V_H-V_L interface. **(A)** The anion-π-π interaction (V_H-D101:V_H-Y100E:V_L-Y49) at the V_H-V_L interface of HCDR3-LFW2. (**B)** The core salt bridge V_H-K94:V_H-D101 and the complex salt bridge V_H-K94: V_H-D101/D102 in V_H-V102D **(C)** Distances between the C_α atoms of V_L-Y49:V_H-Y100E and V_H-Y100E:V_H-D101 residues. Distance values of mutants are plotted together with the WT counterpart to demonstrate the shifts. **(D)** Distances between the O atom of V_H-K94 and N atom of V_H-D101 that is the backbone salt bridge and distances between the N_ζ atom of V_H-K94 and O_δ atom of V_H-D101 that is the side-chain salt bridge for all variants. V_H-V102D mutation is also invented a new ionic interaction with its side chain oxygen atom that competes with the ionic interaction of V_H-D101 oxygen atom, shown as an inset. Color coding follows Figure 1.

A *de novo* salt bridge near the stem of HCDR3 leads to a substantial affinity improvement in V102D

While the improvements in stability in the two V_H-V102 mutants can be primarily traced to a more robust HCDR3-V_L interface, affinity improvements occur mainly through the improved HCDR3-VEGF interactions (**Supplementary Figures 10, 11**). ~~**8, 9).**~~ The V_H-V102D forms a complex salt bridge where one residue forms ionic interaction with more than one residue (**Figure 5B**) [48, 71]. The core salt bridge (V_H-K94:V_H-D101) is accompanied by a mutated aspartate (V_H-K94:V_H-D102). Although the backbone ionic interaction of V_H-K94:V_H-D101 is not disrupted at all, side-chain ionic interactions of V_H-K94 were shared with V_H-D101 and V_H-D102 for both V_H-V102D and V_L-Y49N-V_H-V102D mutants (**Figure 5D**). Forming this complex salt bridge between V_H-K94:V_H-D101/D102 might contribute to the affinity increase for both V_H-V102D and V_L-Y49N-V_H-V102D mutants. The indirect effect of V_H-V102 residue on both affinity and stability through HCDR3 loop conformation is notable and worth investigating.

The complex salt bridge at the stem of HCDR3 improves packing of epitope-paratope interaction

When we checked epitope-paratope interactions, VEGF-I91 is found to be the key player by having an interaction with V_H-H101 of HCDR3 (**Supplementary Figure 17**). ~~**15).**~~ We recognized that V_H-H101:VEGF-I91 interaction might explain drastic affinity changes for affinity improved mutants (V_H-V102D, V_H-V102Y, V_L-Y49N-V_H-V102D, V_L-Y49N-V_H-V102Y) by having less distant interaction overall (**Supplementary Figure 17**). ~~**15).**~~ There are also other important epitope-paratope interactions such as V_H-Y102:VEGF-I80, V_H-Y102:VEGF-G92, V_H-G100:VEGF-R82 (HCDR3-VEGF for all), but no significant difference was observed except for double mutants which have the highest improvements in their VEGF affinities that can be attributed to *de novo* contacts formed between side chains and backbone functional groups (**Supplementary Figure 18, 19**). ~~**16, 17).**~~

To see whether the packing of HCDR3 with VEGF has any contribution to observed affinity, we analyzed the HCDR3 conformation change for V_H-V102D (**Figure 6A**). An angle is calculated to represent tilt of HCDR3 towards VEGF **(Figure 6B).** To measure this angle, two vectors, $\overrightarrow{P_1}$ between the center of masses of scFv and VEGF, $\overrightarrow{P_2}$ between the center of masses scFv and middle residues of HCDR3 (V_H-G100 C_α and V_H-S100A C_α) are used. Θ angle is determined as the cosine angle between those $\overrightarrow{P_1}$ and $\overrightarrow{P_2}$ vectors **(Figure 6B,** **Supplementary Figure 20**). ~~**18).**~~ Scatter plots of calculated θ angle and experimental affinity change showed that there is an obvious correlation for HCDR3 conformation with affinity changes (**Figure 6C**). While mutants with slight affinity increase (V_L-Y49N, V_L-Y49K, V_H-V102Y) are clustered together with angles values very close to that of WT, mutant with the most significant affinity change (V_H-V102D) had more increase from those of all mutants (**Figure 6C**). This might show that the formation of a complex salt bridge at the stem of HCDR3 might alter overall HCDR3 conformation tilting towards VEGF affecting its affinity drastically.

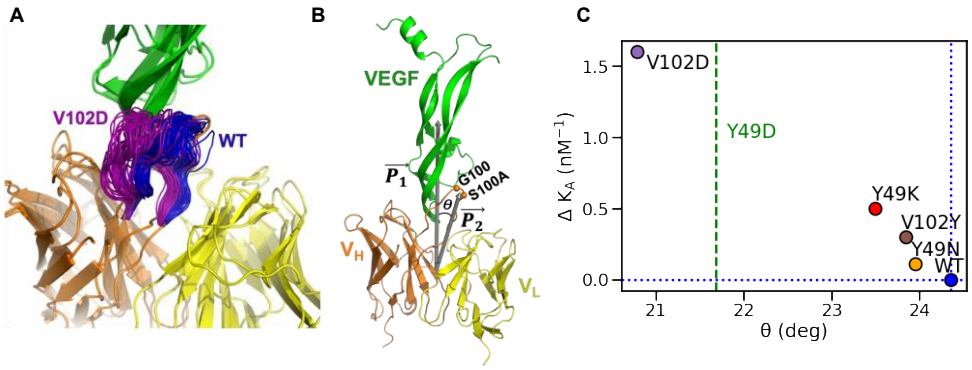

Figure 6: Changes in affinity correlate with a global tilt in HCDR3. **(A)** HCDR3 loop conformations are visualized for WT and V_H-V102D. Alignment is performed based on the reference of the V_H-K94:V_H-D101 salt bridge. HCDR3s are represented as the tubes, HCDR3 frames of V_H-V102D and WT are colored in purple and blue, respectively. **(B)** The cosine angle (θ) change of HCDR3 is calculated between two vectors $\overrightarrow{P_1}$ and $\overrightarrow{P_2}$. $\overrightarrow{P_1}$ vector is the vector between the center of mass of the scFv fragment and the center of mass of antigen VEGF. $\overrightarrow{P_2}$ is the vector between the center of mass of the scFv fragment and the center of masses of V_H-G100 and V_H-S100A C_α atoms. $\overrightarrow{P_1}$ and $\overrightarrow{P_2}$ vectors are colored in gray. Selected atoms are represented as spheres. **(C)** Angle decrease of mutants compared to WT-HCDR3 are scattered through every 100th frame of the whole trajectory (5000 frames). The experimental affinity of the V_L-Y49D mutant could not be obtained, so its representation is made based on our computational results. Color coding follows Figure 1. Distributions of angle of all mutants are shown in **Supplementary Figure 20**. ~~**18.**~~

Field Code Changed

Discussion

Monoclonal antibodies are promising biomacromolecules for various therapeutic and diagnostic applications. However, numerous trade-offs can be encountered during development and improvement stages due to the intrinsic complexity and the structural limited modularity of these molecules [72]. While the antigen affinity is the most natural and crucial developability parameter, its improvement cannot be decoupled from the stability of the antibody in a systematic manner, resulting in an unavoidable affinity versus stability trade-offs [11, 15, 73]. A primary driver of this mutual dependence could lie in the architecture of the HCDR3 region, an elongated loop that forms critical interactions with both the antigen and the antibody light chain.

In this study, we focused on two pivotal residues (Y49 on the light chain and V102 on the heavy chain) that modulate the global orientation of HCDR3 while maintaining its overall shape and structural integrity (**Figure 1**). Of these two residues, the light chain Y49 tolerated a mutation that improved the antigen affinity but a crucial π-π interaction was lost in the V_H-V_L interface, one that proved irreplaceable for the stability. The second residue of focus, heavy chain V102, not only tolerated mutations that reoriented HCDR3 more favorably for antigen binding, but interactions lost with the light chain could be compensated via novel contacts not present in WT. We identified one such mutation, V_H-V102Y, that demonstrated a joint increase in stability and affinity in both our experimental measurements and atomistic molecular dynamics simulations. HCDR3 has two main interfaces, one toward the antigen and the other one spanning part of the V_H-V_L interface. We have

shown that in these mutants (i) the contacts at the HCDR3-VEGF interface increase, resulting in an improved affinity and (ii) the contacts at the HCDR3, LFW2, and LCDR3 region of the V_H-V_L interface increase, probably resulting in an improved stability. These two mutants are direct evidence that HCDR3 is not only important for affinity but also for stability and not necessarily in an antagonistic manner. We note that caution should be taken to avoid drastic trade-offs during affinity maturation efforts on HCDR3. The findings here are a novel proof of concept demonstration with implications for other antibody engineering efforts.

Understanding antibody stability is a more complex issue because the residues contributing to stability are scattered across diverse positions (core domain, surface exposed residues, V_H-V_L interface) [74-77]. In our study, stability increasing mutations (V_H-V102Y and V_H-V102D) showed significantly higher V_H-V_L interface buried surface area (**Figure 4**). This demonstrates the importance of the scope of V_H-V_L packing for the overall antibody stability. In addition, the V_H-V_L orientation is also known to be important for stability [78-81]. In our mutants, no significant correlation was observed between this metric and stability.

It is known that π-π stacking is very important for protein structure and function. Besides π-π, π-cation/amino/anion contacts are also a part of these crucial stacking interactions [82]. Even triple π-stackings are known to contribute to the activity of proteins[83] . In the specific example of light chain Y49, we mutated this residue to collect structural insights into the effect of triple π-stacking interactions at the V_H-V_L interface. We showed that drastic affinity and stability changes occur when the anion-π-π interaction (V_H-D101: V_H-Y100E:V_L-Y49) was mutated through V_L-Y49N/K/D mutations (**Figure 4, 5**). V_L-Y49 is one of the Vernier zone residues. Although Vernier zone residues are by definition not in the CDR regions (but rather usually at the stem of CDRs), they are known to be indispensable for antibody function [24]. These residues are usually back mutated to restore antibody affinity in humanization efforts [84]. Here, we provide further evidence on the importance of Vernier zone residues for antibody engineering efforts [27].

There is a highly conserved salt bridge (V_H-K94:V_H-D101) at the stem of HCDR3 that is critical for HCDR3 to assume its bulge form [85]. If the lysine (or arginine) at position 94 is converted to any other amino acid, HCDR3 loses function due to lack of stabilizing salt bridge and it does not form the bulge [86]. When this salt bridge was converted into a complex salt bridge by V_H-V102D mutation, affinity and stability increased. In-depth analysis of a molecular dynamics simulation of this mutant showed that the complex salt bridge at the stem shifted the HCDR3 loop to tilt towards VEGF, thereby contributing to the affinity increase (**Figure 6**). Even though V_H-V102 is a highly conserved residue in the antibody framework [87], it is nonetheless a potentially interesting locus for future antibody engineering and affinity maturation efforts. As a general approach, V102 might be mutated to "D" or "Y" to increase antibody affinity with no loss or even better stability. Aspartate in this position is very rare (1%), thus immunogenicity should also be considered while designing mutations with rare amino acids in particular positions.

We should also note here the complementarity aspect of our molecular dynamics simulations in understanding the detailed molecular mechanisms associated with the involvement of HCDR3. Hence all the domains of an antibody share the same structural fold [19, 88] and framework residues, especially chosen HCDR3 salt bridge interaction, are usually very conserved among organisms, these findings can be applied to other antibodies in general. The measured energetic differences in the affinities are on the order of a few thermal energies at ambient conditions (as inferred from the dissociation constants), meaning that accurate prediction of protein-protein binding energies is of utmost importance in this context. As an intuitive measure of the relative changes in binding

interfaces, here, we have used pairwise contacts between the epitope and paratope groups. Such geometric metrics are commonly employed in heuristic correlations with experimentally measured energies [89].

Affinity improvement or re-gaining efforts are usually encountered with numerous trade-offs such as loss of stability, lower solubility, and/or higher aggregation propensity, as reviewed elsewhere [11]. Although these *in vitro* properties of a candidate antibody can be co-screened with a variety of experimental tools, scalability is typically costly and cumbersome. In this context, the use of *in silico* tools can alleviate the load by providing precise predictions at a fraction of the cost and time typically invested in an experimental undertaking. In this work, we tapped into the strength of sufficiently long molecular dynamics simulations which not only validated our physico-chemical wet-lab characterization of our mutants but also provided molecular level understanding into the favorable and unfavorable outcomes.

Acknowledgments

This work was supported by the institutional funds of Izmir Biomedicine and Genome Center (IBG) (T.U., S.Kale, and S.Kalyoncu), Council of Higher Education (YÖK) 100/2000 Fellowship Program (M.A.), The Scientific and Technological Research Council of Turkey (TUBITAK)-BIDEB 2211A PhD Achievement Grant (M.A.), and TUBITAK grant 119Z161 (M.A., S.Kale, and S.Kalyoncu). The authors acknowledge the computational resources of TUBITAK ULAKBIM High Performance and Grid Computing Center (TRUBA resources) and the IBG High Performance Computing Facility.

Conflict of Interest

The authors declare that the research was conducted in the absence of any commercial or financial relationships that could be construed as a potential conflict of interest.

Author Contributions

MA, TU, S.Kale and S.Kalyoncu contributed to conception and design of the study. MA carried out *in vitro* experiments. TU and MA carried out *in silico* analysis. TU and MA performed data visualization. MA and TU wrote the first draft of the manuscript. All authors contributed to manuscript revision, read, and approved the submitted version. S.Kale and S.Kalyoncu supervised the project.

References

1. Kaplon H, Muralidharan M, Schneider Z, Reichert JM. Antibodies to watch in 2020. MAbs. 2020;12(1):1703531.

2. Kaplon H, Reichert JM. Antibodies to watch in 2021. MAbs. 2021;13(1):1860476.

3. Bates A, Power CA. David vs. Goliath: The Structure, Function, and Clinical Prospects of Antibody Fragments. Antibodies (Basel). 2019;8(2).

4. Chao G, Lau WL, Hackel BJ, Sazinsky SL, Lippow SM, Wittrup KD. Isolating and engineering human antibodies using yeast surface display. Nat Protoc. 2006;1(2):755-68.

5. Schofield DJ, Pope AR, Clementel V, Buckell J, Chapple S, Clarke KF, et al. Application of phage display to high throughput antibody generation and characterization. Genome Biol. 2007;8(11):R254.

6. Santos J, Cardoso M, Moreira IS, Goncalves J, Correia JDG, Verde SC, et al. Integrated in Silico and Experimental Approach towards the Design of a Novel Recombinant Protein Containing an Anti-HER2 scFv. Int J Mol Sci. 2021;22(7).

7. Goel A, Colcher D, Baranowska-Kortylewicz J, Augustine S, Booth BJ, Pavlinkova G, et al. Genetically engineered tetravalent single-chain Fv of the pancarcinoma monoclonal antibody CC49: improved biodistribution and potential for therapeutic application. Cancer Res. 2000;60(24):6964-71.

8. Fennell BJ, McDonnell B, Tam AS, Chang L, Steven J, Broadbent ID, et al. CDR-restricted engineering of native human scFvs creates highly stable and soluble bifunctional antibodies for subcutaneous delivery. MAbs. 2013;5(6):882-95.

9. Sawant MS, Streu CN, Wu L, Tessier PM. Toward Drug-Like Multispecific Antibodies by Design. Int J Mol Sci. 2020;21(20).

10. Julian MC, Lee CC, Tiller KE, Rabia LA, Day EK, Schick AJ, 3rd, et al. Co-evolution of affinity and stability of grafted amyloid-motif domain antibodies. Protein Eng Des Sel. 2015;28(10):339-50.

11. Rabia LA, Desai AA, Jhajj HS, Tessier PM. Understanding and overcoming trade-offs between antibody affinity, specificity, stability and solubility. Biochem Eng J. 2018;137:365-74.

12. Houlihan G, Gatti-Lafranconi P, Lowe D, Hollfelder F. Directed evolution of anti-HER2 DARPins by SNAP display reveals stability/function trade-offs in the selection process. Protein Eng Des Sel. 2015;28(9):269-79.

13. Faber MS, Whitehead TA. Data-driven engineering of protein therapeutics. Curr Opin Biotechnol. 2019;60:104-10.

14. Cohen-Khait R, Dym O, Hamer-Rogotner S, Schreiber G. Promiscuous Protein Binding as a Function of Protein Stability. Structure. 2017;25(12):1867-74 e3.

15. Julian MC, Li L, Garde S, Wilen R, Tessier PM. Efficient affinity maturation of antibody variable domains requires co-selection of compensatory mutations to maintain thermodynamic stability. Sci Rep. 2017;7:45259.

16. Koenig P, Lee CV, Walters BT, Janakiraman V, Stinson J, Patapoff TW, et al. Mutational landscape of antibody variable domains reveals a switch modulating the interdomain conformational dynamics and antigen binding. Proc Natl Acad Sci U S A. 2017;114(4):E486-E95.

17. Xu JL, Davis MM. Diversity in the CDR3 region of V(H) is sufficient for most antibody specificities. Immunity. 2000;13(1):37-45.

18. Bostrom J, Lee CV, Haber L, Fuh G. Improving antibody binding affinity and specificity for therapeutic development. Methods Mol Biol. 2009;525:353-76, xiii.

19. Chiu ML, Goulet DR, Teplyakov A, Gilliland GL. Antibody Structure and Function: The Basis for Engineering Therapeutics. Antibodies (Basel). 2019;8(4).

20. Herold EM, John C, Weber B, Kremser S, Eras J, Berner C, et al. Determinants of the assembly and function of antibody variable domains. Sci Rep. 2017;7(1):12276.

21. Zhao J, Nussinov R, Ma B. The Allosteric Effect in Antibody-Antigen Recognition. Methods Mol Biol. 2021;2253:175-83.

22. Makabe K, Nakanishi T, Tsumoto K, Tanaka Y, Kondo H, Umetsu M, et al. Thermodynamic consequences of mutations in vernier zone residues of a humanized anti-human epidermal growth factor receptor murine antibody, 528. J Biol Chem. 2008;283(2):1156-66.

551 23. Riechmann L, Clark M, Waldmann H, Winter G. Reshaping human antibodies for therapy.
552 Nature. 1988;332(6162):323-7.

553 24. Foote J, Winter G. Antibody framework residues affecting the conformation of the
554 hypervariable loops. J Mol Biol. 1992;224(2):487-99.

555 25. Wu H, Nie Y, Huse WD, Watkins JD. Humanization of a murine monoclonal antibody by
556 simultaneous optimization of framework and CDR residues. J Mol Biol. 1999;294(1):151-62.

557 26. Safdari Y, Farajnia S, Asgharzadeh M, Khalili M. Antibody humanization methods - a review
558 and update. Biotechnol Genet Eng Rev. 2013;29:175-86.

559 27. Arslan M, Karadag D, Kalyoncu S. Conformational changes in a Vernier zone region:
560 Implications for antibody dual specificity. Proteins. 2020;88(11):1447-57.

561 28. Arslan M, Karadag D, Kalyoncu S. Protein engineering approaches for antibody fragments:
562 directed evolution and rational design approaches. Turk J Biol. 2019;43(1):1-12.

563 29. Tiller KE, Tessier PM. Advances in Antibody Design. Annu Rev Biomed Eng. 2015;17:191-
564 216.

565 30. Zhao J, Nussinov R, Wu WJ, Ma B. In Silico Methods in Antibody Design. Antibodies
566 (Basel). 2018;7(3).

567 31. Izrailev S, Stepaniants S, Balsera M, Oono Y, Schulten K. Molecular dynamics study of
568 unbinding of the avidin-biotin complex. Biophys J. 1997;72(4):1568-81.

569 32. Dogan D, Arslan M, Ulucay T, Kalyoncu S, Dimitrov S, Kale S. CENP-A Nucleosome is a
570 Sensitive Allosteric Scaffold for DNA and Chromatin Factors. J Mol Biol. 2021;433(6):166789.

571 33. Rocco AG, Mollica L, Ricchiuto P, Baptista AM, Gianazza E, Eberini I. Characterization of
572 the protein unfolding processes induced by urea and temperature. Biophys J. 2008;94(6):2241-51.

573 34. Lindorff-Larsen K, Trbovic N, Maragakis P, Piana S, Shaw DE. Structure and dynamics of an
574 unfolded protein examined by molecular dynamics simulation. J Am Chem Soc. 2012;134(8):3787-
575 91.

576 35. Collu F, Spiga E, Chakroun N, Rezaei H, Fraternali F. Probing the early stages of prion
577 protein (PrP) aggregation with atomistic molecular dynamics simulations. Chem Commun (Camb).
578 2018;54(57):8007-10.

579 36. Fernandez-Quintero ML, Pomarici ND, Math BA, Kroell KB, Waibl F, Bujotzek A, et al.
580 Antibodies exhibit multiple paratope states influencing VH-VL domain orientations. Commun Biol.
581 2020;3(1):589.

582 37. Yamashita T. Toward rational antibody design: recent advancements in molecular dynamics
583 simulations. Int Immunol. 2018;30(4):133-40.

584 38. Cheng X, Wang J, Kang G, Hu M, Yuan B, Zhang Y, et al. Homology Modeling-Based in
585 Silico Affinity Maturation Improves the Affinity of a Nanobody. Int J Mol Sci. 2019;20(17).

586 39. Yang B, Lin SJ, Ren JY, Liu T, Wang YM, Li CM, et al. Molecular Docking and Molecular
587 Dynamics (MD) Simulation of Human Anti-Complement Factor H (CFH) Antibody Ab42 and CFH
588 Polypeptide. Int J Mol Sci. 2019;20(10).

589 40. Yoshida K, Kuroda D, Kiyoshi M, Nakakido M, Nagatoishi S, Soga S, et al. Exploring
590 designability of electrostatic complementarity at an antigen-antibody interface directed by
591 mutagenesis, biophysical analysis, and molecular dynamics simulations. Sci Rep. 2019;9(1):4482.

41. Chiba S, Tanabe A, Nakakido M, Okuno Y, Tsumoto K, Ohta M. Structure-based design and discovery of novel anti-tissue factor antibodies with cooperative double-point mutations, using interaction analysis. Sci Rep. 2020;10(1):17590.

42. Zhang YN, Zhang XQ, Zhang XC, Xu JW, Li LL, Zhu XY, et al. Key Amino Acid Residues Influencing Binding Affinities of Pheromone-Binding Protein from Athetis lepigone to Two Sex Pheromones. J Agric Food Chem. 2020;68(22):6092-103.

43. Fernandez-Quintero ML, Kroell KB, Hofer F, Riccabona JR, Liedl KR. Mutation of Framework Residue H71 Results in Different Antibody Paratope States in Solution. Front Immunol. 2021;12:630034.

44. Musafia B, Buchner V, Arad D. Complex salt bridges in proteins: statistical analysis of structure and function. J Mol Biol. 1995;254(4):761-70.

45. Shirai H, Kidera A, Nakamura H. H3-rules: identification of CDR-H3 structures in antibodies. FEBS Lett. 1999;455(1-2):188-97.

46. Weitzner BD, Dunbrack RL, Jr., Gray JJ. The origin of CDR H3 structural diversity. Structure. 2015;23(2):302-11.

47. Tsumoto K, Ogasahara K, Ueda Y, Watanabe K, Yutani K, Kumagai I. Role of salt bridge formation in antigen-antibody interaction. Entropic contribution to the complex between hen egg white lysozyme and its monoclonal antibody HyHEL10. J Biol Chem. 1996;271(51):32612-6.

48. Presta LG, Chen H, O'Connor SJ, Chisholm V, Meng YG, Krummen L, et al. Humanization of an anti-vascular endothelial growth factor monoclonal antibody for the therapy of solid tumors and other disorders. Cancer Res. 1997;57(20):4593-9.

49. Zirlik K, Duyster J. Anti-Angiogenics: Current Situation and Future Perspectives. Oncol Res Treat. 2018;41(4):166-71.

50. Muller YA, Chen Y, Christinger HW, Li B, Cunningham BC, Lowman HB, et al. VEGF and the Fab fragment of a humanized neutralizing antibody: crystal structure of the complex at 2.4 A resolution and mutational analysis of the interface. Structure. 1998;6(9):1153-67.

51. Hudson PJ, Kortt AA. High avidity scFv multimers; diabodies and triabodies. J Immunol Methods. 1999;231(1-2):177-89.

52. Le Gall F, Kipriyanov SM, Moldenhauer G, Little M. Di-, tri- and tetrameric single chain Fv antibody fragments against human CD19: effect of valency on cell binding. FEBS Lett. 1999;453(1-2):164-8.

53. Arslan M, Karadag M, Onal E, Gelinci E, Cakan-Akdogan G, Kalyoncu S. Effect of non-repetitive linker on in vitro and in vivo properties of an anti-VEGF scFv. Sci Rep. 2022;12(1):5449.

54. Fernandez-Quintero ML, Hoerschinger VJ, Lamp LM, Bujotzek A, Georges G, Liedl KR. VH -VL interdomain dynamics observed by computer simulations and NMR. Proteins. 2020;88(7):830-9.

55. Best RB, Zhu X, Shim J, Lopes PE, Mittal J, Feig M, et al. Optimization of the additive CHARMM all-atom protein force field targeting improved sampling of the backbone phi, psi and side-chain chi(1) and chi(2) dihedral angles. J Chem Theory Comput. 2012;8(9):3257-73.

56. Huang J, Rauscher S, Nawrocki G, Ran T, Feig M, de Groot BL, et al. CHARMM36m: an improved force field for folded and intrinsically disordered proteins. Nat Methods. 2017;14(1):71-3.

57. Izadi S, Anandakrishnan R, Onufriev AV. Building Water Models: A Different Approach. J Phys Chem Lett. 2014;5(21):3863-71.

58. Wu TT, Kabat EA. An analysis of the sequences of the variable regions of Bence Jones proteins and myeloma light chains and their implications for antibody complementarity. J Exp Med. 1970;132(2):211-50.

59. Abhinandan KR, Martin AC. Analysis and improvements to Kabat and structurally correct numbering of antibody variable domains. Mol Immunol. 2008;45(14):3832-9.

60. Dunbar J, Deane CM. ANARCI: antigen receptor numbering and receptor classification. Bioinformatics. 2016;32(2):298-300.

61. Van Der Spoel D, Lindahl E, Hess B, Groenhof G, Mark AE, Berendsen HJ. GROMACS: fast, flexible, and free. J Comput Chem. 2005;26(16):1701-18.

62. Humphrey W, Dalke A, Schulten K. VMD: visual molecular dynamics. J Mol Graph. 1996;14(1):33-8, 27-8.

63. Adamczak R, Porollo A, Meller J. Combining prediction of secondary structure and solvent accessibility in proteins. Proteins. 2005;59(3):467-75.

64. Studier FW. Protein production by auto-induction in high density shaking cultures. Protein Expr Purif. 2005;41(1):207-34.

65. Wilkins MR, Gasteiger E, Bairoch A, Sanchez JC, Williams KL, Appel RD, et al. Protein identification and analysis tools in the ExPASy server. Methods Mol Biol. 1999;112:531-52.

66. Lucas X, Bauza A, Frontera A, Quinonero D. A thorough anion-pi interaction study in biomolecules: on the importance of cooperativity effects. Chem Sci. 2016;7(2):1038-50.

67. D'Angelo S, Ferrara F, Naranjo L, Erasmus MF, Hraber P, Bradbury ARM. Many Routes to an Antibody Heavy-Chain CDR3: Necessary, Yet Insufficient, for Specific Binding. Front Immunol. 2018;9:395.

68. Swindells MB, Porter CT, Couch M, Hurst J, Abhinandan KR, Nielsen JH, et al. abYsis: Integrated Antibody Sequence and Structure-Management, Analysis, and Prediction. J Mol Biol. 2017;429(3):356-64.

69. Tan PH, Sandmaier BM, Stayton PS. Contributions of a highly conserved VH/VL hydrogen bonding interaction to scFv folding stability and refolding efficiency. Biophys J. 1998;75(3):1473-82.

70. Masuda K, Sakamoto K, Kojima M, Aburatani T, Ueda T, Ueda H. The role of interface framework residues in determining antibody V(H)/V(L) interaction strength and antigen-binding affinity. FEBS J. 2006;273(10):2184-94.

71. Gvritishvili AG, Gribenko AV, Makhatadze GI. Cooperativity of complex salt bridges. Protein Sci. 2008;17(7):1285-90.

72. Bigman LS, Levy Y. Proteins: molecules defined by their trade-offs. Curr Opin Struct Biol. 2020;60:50-6.

73. Shehata L, Maurer DP, Wec AZ, Lilov A, Champney E, Sun T, et al. Affinity Maturation Enhances Antibody Specificity but Compromises Conformational Stability. Cell Rep. 2019;28(13):3300-8 e4.

74. Worn A, Pluckthun A. Different equilibrium stability behavior of ScFv fragments: identification, classification, and improvement by protein engineering. Biochemistry. 1999;38(27):8739-50.

75. Chang HJ, Jian JW, Hsu HJ, Lee YC, Chen HS, You JJ, et al. Loop-sequence features and stability determinants in antibody variable domains by high-throughput experiments. Structure. 2014;22(1):9-21.

76. Lehmann A, Wixted JH, Shapovalov MV, Roder H, Dunbrack RL, Jr., Robinson MK. Stability engineering of anti-EGFR scFv antibodies by rational design of a lambda-to-kappa swap of the VL framework using a structure-guided approach. MAbs. 2015;7(6):1058-71.

77. Montoliu-Gaya L, Martinez JC, Villegas S. Understanding the contribution of disulfide bridges to the folding and misfolding of an anti-Abeta scFv. Protein Sci. 2017;26(6):1138-49.

78. Worn A, Pluckthun A. Mutual stabilization of VL and VH in single-chain antibody fragments, investigated with mutants engineered for stability. Biochemistry. 1998;37(38):13120-7.

79. Hsu HJ, Lee KH, Jian JW, Chang HJ, Yu CM, Lee YC, et al. Antibody variable domain interface and framework sequence requirements for stability and function by high-throughput experiments. Structure. 2014;22(1):22-34.

80. Tu C, Terraube V, Tam AS, Stochaj W, Fennell BJ, Lin L, et al. A Combination of Structural and Empirical Analyses Delineates the Key Contacts Mediating Stability and Affinity Increases in an Optimized Biotherapeutic Single-chain Fv (scFv). J Biol Chem. 2016;291(3):1267-76.

81. Warszawski S, Borenstein Katz A, Lipsh R, Khmelnitsky L, Ben Nissan G, Javitt G, et al. Optimizing antibody affinity and stability by the automated design of the variable light-heavy chain interfaces. PLoS Comput Biol. 2019;15(8):e1007207.

82. Dalkas GA, Teheux F, Kwasigroch JM, Rooman M. Cation-pi, amino-pi, pi-pi, and H-bond interactions stabilize antigen-antibody interfaces. Proteins. 2014;82(9):1734-46.

83. Klein BJ, Vann KR, Andrews FH, Wang WW, Zhang J, Zhang Y, et al. Structural insights into the pi-pi-pi stacking mechanism and DNA-binding activity of the YEATS domain. Nat Commun. 2018;9(1):4574.

84. Haidar JN, Yuan QA, Zeng L, Snavely M, Luna X, Zhang H, et al. A universal combinatorial design of antibody framework to graft distinct CDR sequences: a bioinformatics approach. Proteins. 2012;80(3):896-912.

85. Decanniere K, Desmyter A, Lauwereys M, Ghahroudi MA, Muyldermans S, Wyns L. A single-domain antibody fragment in complex with RNase A: non-canonical loop structures and nanomolar affinity using two CDR loops. Structure. 1999;7(4):361-70.

86. Al-Lazikani B, Lesk AM, Chothia C. Standard conformations for the canonical structures of immunoglobulins. J Mol Biol. 1997;273(4):927-48.

87. Wang N, Smith WF, Miller BR, Aivazian D, Lugovskoy AA, Reff ME, et al. Conserved amino acid networks involved in antibody variable domain interactions. Proteins. 2009;76(1):99-114.

88. Janeway CA Jr TP, Walport M, et al. The structure of a typical antibody molecule. Immunobiology: The Immune System in Health and Disease 5th edition. New York: Garland Science; 2001.

89. Vangone A, Bonvin AM. Contacts-based prediction of binding affinity in protein-protein complexes. Elife. 2015;4:e07454.

Credit Author Statement

MA, TU, S.Kale and S.Kalyoncu contributed to conception and design of the study. MA carried out *in vitro* experiments. TU and MA carried out *in silico* analysis. TU and MA performed data visualization. MA and TU wrote the first draft of the manuscript. All authors contributed to manuscript revision, read, and approved the submitted version. S.Kale and S.Kalyoncu supervised the project.